Numerical modeling of 3D woven composite reinforcements: A review

Yanneck Wielhorski, Arturo Mendoza, Marcello Rubino, Stéphane Roux

Numerical modeling of 3D woven composite reinforcements: A review

Yanneck Wielhorski[a,*], Arturo Mendoza[b,c], Marcello Rubino[a,b], Stéphane Roux[b]

[a] *Safran Aircraft Engines, Rond-point Réné Ravaud - Réau, 77550 Moissy-Cramayel, France*
[b] *LMT (ENS Paris-Saclay/CNRS/Univ. Paris-Saclay), 4, Avenue des Sciences, 91192 Gif-sur-Yvette, France*
[c] *Safran Tech, Rue des Jeunes Bois, 78772 Magny-les-Hameaux, France*

Abstract

The literature of numerical modeling of 3D woven composite reinforcements shows that a wide range of impressive studies have been carried out in the last two decades. During this period, two distinct strategies have emerged: the *predictive* approaches that call for a mechanical construction as well as numerical simulations (*e.g.*, FE method), and the *descriptive* approaches that are devoted to extracting the geometry of a real textile from micro-tomographic images. In the former methods, different geometrical and mechanical strategies have been employed for mimicking the yarn behavior at either the meso- or sub-mesoscales. And in the latter ones, different approaches ranging from *ad hoc* image processing pipelines up to more advanced machine learning strategies have been used but only at the mesoscale. This paper aims to highlight the advantages and ideal usecases of each method as well as for each analysis scale (meso- or sub-mesoscale). A common terminology is proposed for organizing and discussing the various meso- and sub-mesoscale strategies. It should be noted that this work only covers the modeling strategies for the textile reinforcement (*i.e.*, dry fabric), thus meso- or macroscale analyses of complete composites are not discussed.

Keywords: Textile modeling, Woven fabrics, Composite materials

1. Introduction

The rapid growth of woven composite materials in many industries is a testimony of their excellent mechanical properties. Indeed, woven composites have appeared in new applications requiring high *specific* properties (*e.g.*, strength to weight ratio). Some examples of their use in the aeronautics, automotive and naval industries are: the composite fan blades and fan case in the LEAP engine that provide superior damage tolerance and increased aerodynamics [1], composite automotive structural parts that reduce fuel consumption while maintaining high resistance and rigidity [2], and composite bridge deck with increased resistance to corrosion and fatigue [3].

This is particularly important for 3D woven composite materials, since they can be used for manufacturing complete components with complex 3D shapes. Indeed, the manufacturing process does play an important role in defining the mechanical behavior of the composite since each of the steps could modify (to different degrees) the structure of the reinforcement [4]. These steps include the main processes of weaving, forming and molding, as well as some manual intermediate steps (*e.g.*, draping). Moreover, by (locally) customizing their three-dimensional weaving pattern [5], they can be engineered to present targeted behaviors to complex loads [6, 7]. These characteristics have helped in widening their use.

Commonly, computations at the scale of the part are performed using local descriptions of the material properties (*e.g.*, stiffness, permeability) but not their detailed structure so as to considerably reduce overall computational cost. Hence, decent calculations on parts with complex shape and large size are possible.

*Corresponding author.
Email address: yanneck.wielhorski@safrangroup.com (Yanneck Wielhorski)

This approach, called homogenization, refers to the process of replacing multi-phase material properties and a known detailed geometry by a simpler equivalent single-phase material over a Representative Volume Element (RVE). The change from a finer scale to a coarser one usually relies on homogenized constitutive laws relating average fields (*e.g.*, strain, stress, pressure, fluid flow) [8].

Homogenization techniques applied on 3D woven composites have been successful in showing failure and damage initiation at the lower scales while also highlighting the in-plane and out-of-plane mechanical properties [9, 10]. However, they have been shown less well suited for modeling the progression of failure or damage since they cannot capture the local variations in the stress state resulting from the internal architecture [11, 12] (*e.g.*, fiber matrix decohesion, fiber breakage). Thus, in order to account for the intrinsic heterogeneous nature of composites (*e.g.*, highly anisotropic behavior), homogenization techniques require a rich underlying nonlinear continuum theory [13].

In such a manner, numerical modeling at the mesoscopic scale (mesoscale for brevity) provides better design and analysis capabilities by providing an accurate description of these complex internal geometrical features. Mesoscale modeling seeks a faithful description of the textile reinforcement (and possibly matrix constituent) so as to characterize and predict their final physical properties and behavior. Here, the multiscale nature of the composite (fiber, yarn, textile, composite) [14] is not only acknowledged but also taken into consideration. In particular, the spatial modeling of the textile geometry focuses on capturing a good "mean" behavior of the entire fabric, as well as obtaining a faithful characterization of the yarn variability (*e.g.*, thickness, width, spacing [15]), making a compromise between the modeling accuracy and the computational cost [16].

Amongst the various modeling strategies, two main distinct philosophies (categories) can be distinguished: the **predictive** and the **descriptive** ones. On the one hand, the **predictive** approaches are based on a nominal (idealized) geometry of the textile. These methods demand varying degrees of knowledge on the (fiber and) yarn mechanical behavior (*e.g.*, constitutive laws) since they resort to numerical simulations that aim at representing (more or less faithfully) the physical phenomena participating in the manufacturing process (*e.g.*, compression and bending of yarns and their rearrangement). They are the preferred method for textile modeling, insomuch as they are implemented in Textile Geometry Pre-Processors (TGP) packages such as WiseTex [14], TexGen [17] or Textile Generating Software (TGS) such as MultiFil [18].

On the other hand, the **descriptive** strategies characterize a *real* textile using image processing techniques on X-ray tomographic images (which allow observing inside the material). This acquisition method usually requires a precise calibration so as to provide 3D images with sufficient contrast and spatial resolution for segmenting the yarn structures [19, 20]. While this methods can provide a very detailed geometry of a woven part, some effort is required in order to allow for generalization to variants of the material (*e.g.*, different compaction levels).

It is worth mentioning that the aforementioned classification of approaches into predictive and descriptive ones is a novel contribution of this work. Indeed, previous reviews on this matter do not require such vocabulary as they have mainly focused on only one of these strategies. For example, while Lomov et al. [14], Ansar et al. [21] and Gereke and Cherif [22] reviewed works on predictive methods, Naouar et al. [23] did so for descriptive ones. Additionally, the present review paper will gather state-of-the-art methods, which call for more advanced computing techniques than those previously cited reviews.

The article is structured as follows. Section 2 presents a general overview of 3D woven fabrics and highlight the particular features of 3D woven composites. Similarly, section 3 focuses on the yarn, a central element of interest for every modeling strategy. It also presents some general concepts that intend to unify the variety of ideas employed in the literature. Next, in sight of the diverse nature of these approaches, the details of each of the descriptive and predictive strategies found in the literature are provided in sections 4 and 5, along with an analysis of their advantages and limitations. Moreover, summary tables and charts are provided so as to allow for swift comparisons between the many approaches. These two sections constitute the main contribution of this paper. Finally, section 6 provides some concluding remarks.

2. 3D woven interlock fabrics: an overview

Multi-layer 3D woven reinforcements are obtained by the textile process of weaving (in contrast with other textile techniques such as braiding, stitching and knitting) [21, 24, 25]. This process consists in interlacing yarns following a weaving pattern. The latter is defined over a unit cell and tiled most often periodically along two orthogonal directions, warp and weft, in the weaving plane. Then, as the warp yarns (those inserted along the warp orientation) are fed into the Jacquard loom through the heddles, a selection of those is selected and lifted following the weaving pattern [26]. This process creates a space (between warp yarns) into which the weft yarns are inserted (orthogonally) by means of a weaving shuttle. The reed (a device resembling a comb) is then used to separate and space the warp yarns across the width of the fabric and to press the weft yarns (also known as fill or pick yarns) against the already woven part.

During the weaving process, the binder yarns (also called z-yarns), usually placed along the warp orientation, are introduced through the thickness so as to reinforce the textile. This feature considerably lessens the delamination phenomena [27] since they interlock the remaining (non interlaced) yarns. It should be noted that the binder yarns are not necessarily different from the others but often do present a lower fiber count. Also, if the weaving pattern is designed as such, all yarns in a given orientation (*e.g.*, warp) can behave as binder yarns. These 3D woven preforms with only three yarn sets (warp, weft and binders) are called **interlock fabrics** [28].

Moreover, the number of interlocked layers divides woven preforms into *through-the-thickness* interlock and *layer-to-layer* interlock (also called ply-to-ply interlock). While binder yarns interlace all the layers in a through-the-thickness interlock, they only interlace one or a few layers at a time in a layer-to-layer interlock (*e.g.*, 5-layer interlock). Similarly, the binder yarn undulation divides woven preforms into *angle-interlock* and *orthogonal-interlock*.

This undulation angle (measured with respect to the horizontal weaving plane) is a right angle for orthogonal interlock fabrics. In this case, the binder yarns "cut across" the textile in the thickness direction. On the contrary, when the binder yarns interlace more than one column simultaneously, the fabric is an angle interlock one (acute undulation angle).

By combining the two previous segmentation schemes [21], 3D interlock composites can be categorized into four categories. However, given that no layer-to-layer orthogonal interlock composites were found in the literature covered by the present paper (numerical modeling), only the three other categories are considered. Figure 1 shows the configurations for the different interlock patterns along with the references in which they are studied. Based on the number of published literature, the orthogonal through-the-thickness interlock type is the one that has received the most attention in the numerical modeling community. In general, the through-the-thickness interlock architecture has been well studied [27], notably for its tensile and compressive behavior.

Furthermore, a feature of interest of some textile preforms is the satin, essentially a two-dimensional weave on the surface of the fabric that differs from the bulk one [29]. Surface weave yarns are generally incorporated into the structure so as to provide a smooth fabric surface. As such, they contribute the least to the mechanical properties of the composite but protect the core textile from surface damage that is susceptible to occur during processing or service. This is yet another example of the customization that 3D weaving composites offer.

Once the textile reinforcement has been woven, the forming and matrix injection processes follow. As its name suggest, the forming process of reinforcements consists in shaping the "flat" textile into its "final" 3D shape. For particularly complex shapes, the forming process is a crucial step, since it could lead to undesired weaving defects such as waviness, wrinkles or locking [13, 30, 31]. Then, the matrix is added using one of the many processes of Liquid Composite Molding family [32, 33, 34] (*e.g.*, Resin Transfer Molding or Vacuum-Assisted Resin Transfer Molding). Finally, according to the type of matrix employed, 3D woven composites can be categorized into organic matrix composites (OMC) [35] or ceramic matrix composites (CMC) [36].

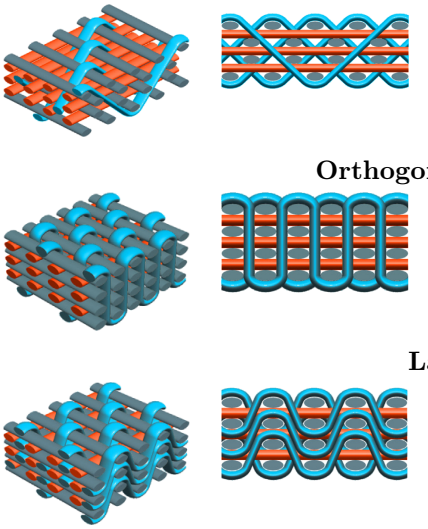

Through-the-thickness angle interlock

2000-2010 [14, 37, 38, 39]
2011-2015 [40, 41, 42, 43, 44]
2016-2021 [27, 45, 46, 47]

Orthogonal through-the-thickness interlock

2000-2010 [26, 37, 48, 49]
2011-2015 [11, 31, 40, 42, 44, 50, 51, 52, 53, 54, 55]
2016-2021 [5, 12, 27, 46, 47, 56, 57, 58, 59, 60, 61, 62, 63, 64, 65]

Layer-to-layer angle interlock

2000-2010 [9, 37, 39, 66, 67, 68]
2011-2015 [40, 52]
2016-2021 [18, 27, 46, 47, 65, 69, 70, 71, 72, 73, 74, 75]

Figure 1: Configurations for interlock types (graphics from Gereke and Cherif [22]) and segmentation of literature by year of publication

3. Yarns: physical features and modeling strategies

The goal of textile modeling is to provide a faithful spatial description of the yarns. This includes the yarn path (also known as yarn center line) as well as the associated cross sections all along the yarn. The former is usually modeled as a 3D curve and the latter as 2D shapes on planes perpendicular to the yarn path tangent. The determination of both yarn path and cross section is essential since they play an important role in the mechanical properties of the woven preform. For example, a correct calculation of the out-of-plane crimp depends on an accurate prediction of the yarn path [14]. Similarly, a faithful prediction of yarn cross section deformations will allow for a precise estimation of the intra-yarn fiber volume fraction [50, 56, 74, 76].

In sight of the complexity introduced by the fibers, describing the yarn can be done either at the **mesoscale** or at the **sub-mesoscale**. While mesoscale modeling aims at capturing the phenomenology of the yarn behavior by considering geometrical or physical constraints, the sub-mesoscale modeling resorts to describing the behavior of the constituting fibers, or more precisely, the behavior of "virtual fibers", an abstraction of fiber bundles that will be discussed below. In both cases, the aim is to properly capture the yarn deformations within the textile, either by employing "complex" formulations for the yarn cross section (mesoscale modeling) or by employing smaller entities (sub-mesoscale modeling) with simple constitutive laws and interactions but whose collective behavior reproduces that of the yarn.

Some studies are devoted to modeling the yarn without any consideration for the "real" physical behavior. In such **surrogate** methods, the purely geometrical (the oldest one) [17, 77, 78] and hollow tube modeling [16] could be mentioned. These alternative approaches allow one to describe the yarn behavior as accurately as possible without requiring complex identification of the yarn deformation modes.

It is noteworthy that the mesoscale geometrical model can also form the basis for the **mechanically based** models [38, 79, 80], aiming to identify each of the yarn deformation modes that take place during the manufacturing processes. Indeed, these mechanical methods are usually based on the purely geometrical ones, as they provide the initial textile configuration. In this context, the yarn is represented as a continuum media for which the mechanical properties are not derived from the lower scale but rather from a top-down approach. Within this latter, general considerations such as "mechanical objectivity" or frame indifference are used together with postulated simplifying assumptions [38]. Examples of such assumptions are the absence of coupling between different deformation modes, or polynomial expansion of the mechanical response along

specific strain directions. In such an approach, mechanical properties have to be identified from tests, as if they were the fundamental constituents [80, 81, 82].

In the sub-mesoscale approach, it is natural to envision the mechanical behavior of yarns as resulting from a homogenization of its elementary constituents (the fibers). However, a textile simulation taking into account the behaviors of *all fibers* (typically 10^4 to 10^5 fibers per yarn), as well as their interactions, is unfeasible since the computational cost would be prohibitive. To get around this issue, a micromechanical approach was introduced: the yarns are described by a bundle of **virtual fibers** each "grouping" many real fibers [83, 84, 85, 86, 87]. This simple idea brings down the "prohibitive calculation" into a more manageable one.

Such simulations, while "simpler" than a complete one, still need to solve the many contact interactions between virtual fibers [18, 83]. Indeed, a direct comparison between methods is not possible since varying either the number of degrees of freedom for the constitutive laws (mechanically based) or the number of virtual fibers for sub-mesoscale model would change the computational time gap. So, the merit of this approach is a realistic description of the fibers and possibly their interactions but the main drawback is the high cost due to the complex determination of contacts and friction. This branch of mechanics, that deals with infinite stiffness contrasts (rigid cross sections, inextensible fibers, but null tangent stiffness of frictional forces in the slip regime) is called "non-smooth" mechanics [88, 89], is very challenging numerically and leads to a strong motivation to go to fewer fibers.

Overall, the rationale behind this approach is the following: an infinite number of fibers leads to a well-defined continuum model, where the number of fibers no longer plays a role. Thus, even with much fewer "equivalent" fibers (*i.e.*, grouping elementary fibers together into bundles), the asymptotic continuum regime may be very accurately reproduced. Hence, a very good picture of the yarn behavior can be achieved at low cost.

Finally, the choice of method should be made with regards to the trade-off between a desired geometrical and mechanical precision and an accessible computing time, according to the purpose of the simulation.

3.1. Physical description

While at the mesoscale, the yarn is the elementary entity of the textile reinforcement, at a sub-mesoscale (microscale) it can no longer be seen as such (a *single* entity). Indeed, a yarn is composed of an assembly of many unidirectional fibers, also called filaments. The number of fibers for typical yarns is in the order of thousands or tenths of thousands (*e.g.*, 6k=6,000 fibers, 12k [50] or 48k [18]).

The overall yarn mechanical behavior is defined by that of the individual fibers, as well as the internal cohesion forces acting on them. It has been shown that understanding internal yarn cohesion forces is paramount to properly model the yarn mechanical behavior [17, 90, 91, 92]. Indeed, the two factors that contribute to this cohesion, the internal fiber arrangement and the sizing agent, need to be studied.

The sizing agent is a coating that, when applied to the fibers, allows them to stick to each other at the microscale and protects them from friction damage [93]. Hence, it prevents internal fiber slippage as well as yarn fraying during yarn deformation [94]. Besides, wear of the sizing layer could change the friction force and therefore the surface state of the fiber [94, 95]. Tourlonias et al. [93] showed that the greater the wear of sizing layer, the lower the coefficient of variation. Many recent studies are devoted to quantify inter-tow frictional behavior including notably effects of the angle on the tow-tow friction coefficient [95, 96]. Moreover, Wu et al. [97] have studied the effect of normal load on the frictional and wear behavior of carbon fiber by simulating the tow-on-tool friction relevant to the beating-up motion of three-dimensional weaving process. They showed that the coefficient of friction increases with the increase of normal loads.

Yet, the sizing agent alone is not strong enough to prevent the yarn to be separated into individual fibers or bundles of fibers when the yarn section is compressed. Hence, yarns can be twisted so as to encourage a better yarn cohesion (see figure 2). Indeed, a high twist factor will stiffen the yarn since it will experience less flattening under lateral pressure [90, 98]. Note that the range of the twist factor could be wide: from 20 [18] to 55 [64] and even 410 [99] turns (twists) per meter (tpm). However, it will also induce irreversible deformations of yarn cross section due to increased cohesion as fibers are pressed against each other (specially under tension) [100].

(a) 1-ply (b) 3-ply

Figure 2: Synchrotron images of yarns from Sibellas et al. [99]

In some works, the yarn is referred to as tow before twisting (*i.e.*, a tow is a bundle of continuous untwisted fibers) [14, 43, 67, 101]. Moreover a yarn can be composed of multiple tows twisted together (the individual tows are not twisted). In such case, the yarn is known as n-ply, where n denoted the number of tows that compose it [99].

It is important to note that the yarn twist generates the migration of the outer plies towards the core of the yarn section [102], along with a diverse distribution of fiber orientations. Not only this favors strong heterogeneity of the local fiber orientation within plies, but also the local distribution of fibers orientation evolves with the distance to the yarn axis.

In addition to the fiber orientation, the fiber geometry (aspect ratio, cross section, waviness) and the amount of fibers have been shown to have an impact on micro-mechanisms that induce yarn deformation [99, 103, 104]. They, along with the intra-yarn fiber volume fraction (also called fiber packing density [105]), have a direct impact on the many contact features which include the number of contact interactions, their orientation, their spatial distribution, and the geometry of the contact surface [103]). These considerations further highlight the nonlinear response observed during yarn compression [103] or tension [104].

Badel et al. [38] obtained covariograms of the spatial distribution of yarn fibers on a deformed reinforcement (after shearing or biaxial tensile tests) since the significant initial dispersion of the fiber distribution in the undeformed state make the covariograms unusable. They note that a sample can be assumed isotropic when the covariograms look alike in both directions (of the cross sectional images). The observed quasi-homogeneous distribution of fibers validates the mechanical assumption of transverse isotropy. However, this is a necessary but not sufficient condition since the case of a twisted yarn invalids the mirror symmetry with respect to a plane including the yarn longitudinal axis.

3.2. Surrogate modeling

Surrogate models propose representations that can be seen as analogous to actual yarn behavior. Hence no physical foundations are explicitly needed. Two main surrogate methods are to be considered: geometrical modeling and a technique based on hollow tubes. While the former attempts to describe yarn body (yarn path and shape cross section variations) using purely geometrically features, the latter relies on an artificial shrinking and dilation of the yarn cross section under a fluid flux simulation.

3.2.1. Geometrical description

Multiple strategies exist for constructing mathematical models that describe the yarn. The objective here is to provide an "usable" 3D model that captures the yarn as it evolves along the textile. Constructing such model requires [91]: (i) a representation of the yarn path, (ii) a description of the cross section, and (iii) a meshing strategy. Concerning the first and second elements, the notion of interpolations schemes and parametrization functions is paramount. Their use allows to reduce the number of control points (variables) required for describing the desired shapes. Then, given that most applications need the 3D model in the form of a 3D mesh (either surface or volume), the third step is usually a required post-processing one. The complexity of this final step is directly related to the approaches followed for obtaining the 3D model.

The **yarn path** can be seen as a parametric function that outputs a 3D position for a given curvilinear distance along the yarn. The most general approach for representing a yarn path is to specify a (discrete) set of master points (also called master nodes or control nodes) [11, 17, 42, 106], and interpolate between them.

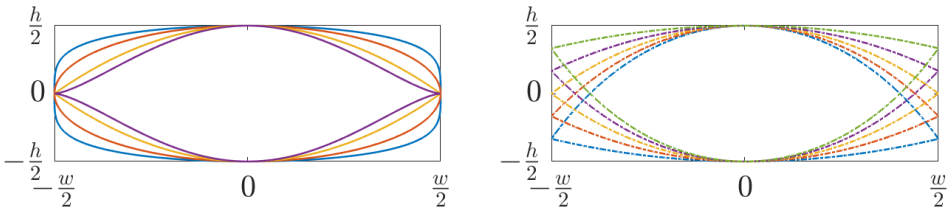

(a) (b)

Figure 3: Analytical yarn cross sections of width w and height h modeled (a) using a power ellipse with exponents $[0.5, 1, 2, 3]$ (from blue to purple), and (b) with a lenticular shape with distortion distance $[-h/3, -h/6, 0, h/6, h/3]$ (from blue to green)

One of the most common interpolation schemes employed are spline functions. A spline is a curve that is formed from a collection of simple segments connected end-to-end. These segments are polynomial functions with defined boundary conditions (*e.g.*, periodicity of the curve) so that their junctions are fairly smooth (*i.e.*, C_1 continuity for cubic splines). Different methods for defining these boundary conditions have been explored: cubic Bézier splines, natural cubic splines, and periodic cubic splines [17, 42, 61, 67, 107]. From those, Bézier splines (B-splines) are the most popular [91].

Alternatively, a combination of sinusoidal curves and segment lines [77, 98, 108, 109] or a cubic polynomial curve [110] have also been employed for describing the yarn path. However, spline curves are preferred to polynomial ones. Not only they can achieve similar results for low order polynomials, but they also avoid the undesired oscillations that occur at the curve boundaries for high order polynomials [17].

Nonetheless, it should be noted that splines can also be sensitive to initial conditions. Hence, small perturbations to the master points may lead to drastically different paths. A simple strategy proposed for alleviating this problem consists in inserting two adjacent points (before and after) any master point [91].

Generally, a yarn **cross section** is a closed 2D shape anchored to a master point of the yarn path. These shapes are embedded in a plane orthogonal to the yarn path. They can also be described using a set of points and interpolation functions (*e.g.*, closed polygons [106] or spline curves). However, the most common approach is to employ parametric functions to describe them [108]. These include common (algebraic) curves such as circles [77, 107, 108], rectangles [14, 66], ellipses [14, 17, 61, 66, 77, 78, 108]. Geometrical shapes such as racetrack shapes [77, 111] (also known as a stadium shape), (convex) power ellipses [17, 112] or lenticular shapes [14, 17, 66, 112, 113] have also been proposed (see figure 3 for the latter two cases).

It is important to note that, while some works employ constant cross sections along the yarn [77, 114], other studies have shown that this assumption is not valid for most cases [42, 90, 98, 115]. Similarly, few observations have shown cross sections to be dissymmetric from top to bottom [113]. Hence, the lenticular shapes can be particularly attractive since they can be made to display this type of bottom-top dissymmetry [17, 116] (see figure 3) whereas they remain left-right symmetrical (vertical direction).

Finally, different **meshing strategies** can be employed for obtaining the complete yarn model. The simplest approach consists in sweeping a predefined constant cross section along the yarn path [77, 109] as it can be seen in figure 4. If this cross section is previously meshed, it will provide a volume mesh of the yarn [114]. An improvement over this method consists in connecting consecutive cross sections by building triangular or rectangular surface facets between control points. However, this approach requires that the cross sections have the same number of points. Furthermore a more advanced approach is to interpolate between consecutive cross sections using linear or cubic interpolation functions [17, 117]. As can be seen in figure 5, this latter approach can even be applied between cross sections of different shapes.

3.2.2. Hollow tubes

Stig and Hallström [16] developed the so called **hollow shell method**, in which the yarn is described as a tube with transversely isotropic walls (see figure 6). These initial tubes are obtained using the TGP TexGen [17] that provides the idealized yarn paths. Moreover, the authors note that these initial yarn

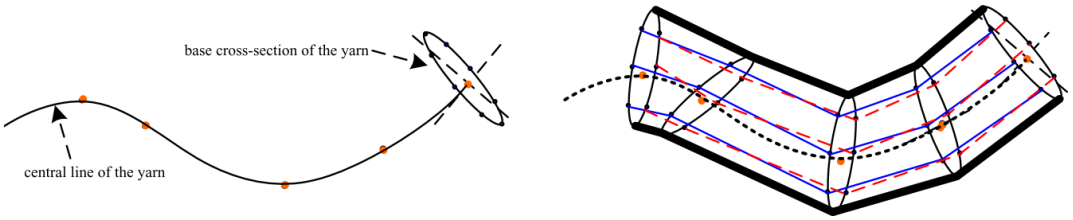

Figure 4: Yarn modeling based on sweeping the cross section along its path from Liao and Adanur [77].

Figure 5: Results from Priyanka et al. [117] for interpolation between ellipse, lenticular, power ellipse and rectangular shapes assigned at each yarn node (from left to right)

trajectories do not appear to influence the final textile architecture significantly.

The hollow tubes that compose this geometrical model are first shrunk. As such, the now smaller circular yarn cross sections guarantee that no yarn inter-penetration occurs. Then, an explicit FE model, similar to a fluid flux simulation, under general contact conditions is employed for expanding the yarns until they satisfy the desired average yarn volume fraction (using the average global and intra-yarn fiber volume fractions). A constant fluid flux is chosen for the yarn expansion, increasing the volume of the tubes linearly at low rate avoiding inertia effect.

As figure 7 shows, the resulting model successfully captures the yarn deformations. Note that radial expansion is obtained by conferring a low transverse stiffness to the tubes. This is obtained by ensuring that the longitudinal Young's modulus is considerably more prominent than the transverse properties. Moreover, the tube walls need to be thick enough and the shear stiffness small enough to prevent local buckling.

3.3. Mesomechanical models

While surrogate modelings as such geometrical approaches or hollow tubes attempt to depict the yarn shape without actual physical foundations, the classical continuum mechanics (Cauchy material) could be introduced by modeling a **realistic yarn behavior**. Nevertheless, this is still not a complete model since it does not take into account all couplings between fibers rigidities and interactions inside the yarn body. In reality, the yarn has plastic deformations but, due to the complexity of phenomena involved, most approaches choose to work within the elastic theory framework and thus reduce the number of degrees of freedom required. This continuum approach for mechanical behavior is based on constitutive equations able to cope with the large displacements and large strains that yarns exhibit (*i.e.*, finite strain theory). These

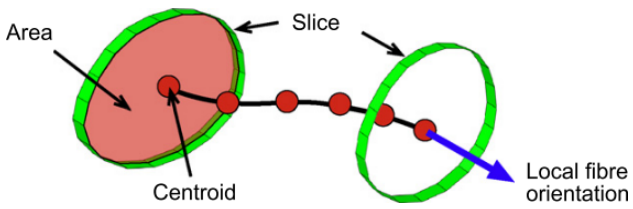

Figure 6: Two slices of a strand from the tube model from Stig and Hallström [118].

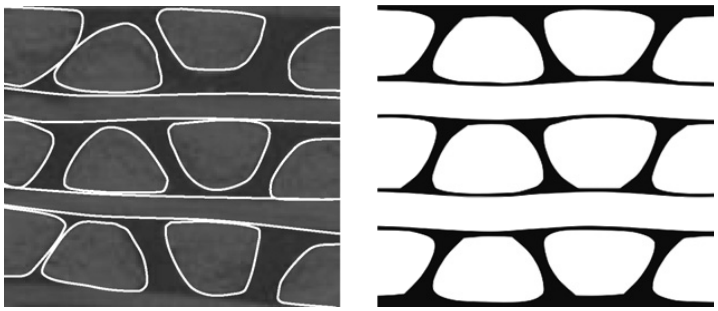

(a) (b)

Figure 7: Results from Stig and Hallström [16], comparison between (a) a CT scan of a dry weave sample, and (b) the corresponding section in obtained FE model

include two relevant constitutive law families: hyper- and hypo- elastic formulations [30, 38, 79, 80, 119, 120, 121, 122, 123, 124].

On the one hand, a **hyper-elastic** formulation is based on a strain energy density, which is a potential from which the stress can be computed, and guarantees thermodynamic consistency (energy conservation and no dissipation). As a result, energy and stress are independent of the strain history. On the other hand, the **hypo-elastic** formulation is based on an incremental formulation where the stress rate is related to the strain rate. Such laws are easy to formulate, and to adapt. However, they come with no guarantee of thermodynamic consistency and may exhibit a strain history dependence.

In both approaches, two fundamental pillars must be followed. First, the deformation modes that the constitutive equation has to depict [123] are to be identified. And second, they must fulfill the principle of material indifference. Hence, relationships between objective quantities need to be expressed, these are independent of the observer and the framework in which it is applied.

Elasticity in the nonlinear range must be established in terms of a hyperelastic strain energy potential [79, 125]. The formulation of **hyper-elastic** laws implies that the free energy per unit volume of the reference configuration can be represented as a function of the deformation gradient and as such it respects the material objectivity condition [120]. In the large displacement/small strain case, the linear constitutive equation can be expressed through the second Piola–Kirchhoff stress tensor which is the derivative of the elastic strain energy potential with respect to the right Cauchy-Green strain tensor. Bonet and Burton [79] presented a transversely isotropic hyperelastic functional that can be used for large strain applications.

To satisfy the existence of a strain energy, two conditions on the strain energy function are required: its quasi-convexity and its coercivity. Indeed, in order to guarantee the existence of solutions in large strain elasticity, the free energy function has to be convex or quasi-convex [126]. However, due to the difficulty to prove the quasiconvexity condition, a stronger one of polyconvexity has been introduced by Ball [127]. Then by ensuring, the polyconvexity of the strain energy function, each energy term related to the deformation gradient (*i.e.*, deformations of line, surface and volume) have to be convex. This notion of convexity of the strain-energy function is very important, since it guarantees a physically meaningful mechanical behavior. This polyconvex strain energy functions could hence *a priori* satisfy the condition of the stress-free natural state [126].

The strain energy of an orthotropic law must only depend on strain tensor invariants to satisfy the condition of material symmetry. For instance, the strain-energy function of an isotropic hyper-elastic material can be expressed as a scalar-valued function of the three principal invariants of the Cauchy-Green deformation tensor according to the tensor function representation theorems [128]. For a transversely isotropic material, the strain energy is dependent upon two additional invariants related to the main fiber direction captured in the structure tensor [79]. Unsurprisingly, all approaches found in the literature model the yarn with a transversely isotropic behavior (although this choice is incompatible with yarn twisting).

Charmetant et al. [80] proposed the idea to relate these five standard invariants of the strain energy with

four "physically-based" invariants related to uncoupled deformation modes of the yarn (see figure 8). These describe the preferred directions (local orientations) of the material in: (i) elongation and (ii) shear along the yarn direction, as well as (iii) compaction and (iv) shear in the transverse direction (*i.e.*, of the yarn cross section). Despite probable couplings between deformation modes, the complete strain energy function is postulated to be equal to the sum of the strain energy of each deformation mode for the hyper-elastic law [80]. Although this law has mechanical and thermodynamical soundness, its constitutive parameters need to be identified from experiments performed at the mesoscale (because the law is not derived from an up-scaling procedure). The low symmetry of yarns (even ignoring their chiral character) implies a large number of invariants and an exponential growth of constitutive parameter numbers with the order of the polynomial expansion of the free energy in those parameters. Since these constitutive parameters need to be identified experimentally, coupling of modes with high order polynomials leads to an un-affordable number (and complexity) of mechanical tests. This is also a strong argument for postulating decoupling between different modes, although this is not motivated by first principles, nor experimental observations.

Additionally, the Taylor (polynomial) expansion for the hyper-elastic formulation does not consider asymptotic behaviors. Yet, this type of behaviors is characteristic of many important quantities such as the limit density of fibers inside the volume (*i.e.*, maximum fiber volume fraction). Hence, accounting for the maximum surface deformation will require a very large number of terms, and a very slow convergence to the asymptotic regime.

In a **hypo-elastic** formulation, the objective Cauchy stress *rate* is related to the strain *rate* by a fourth order hypo-elastic tensor which depends on either stress or strain [129]. Here, one of the main difficulties is the choice of a suitable objective stress rate. This problem of objectivity stems from the difficulty of following the anisotropic (even orthotropic) directions. Indeed, the derivative with respect to time of an objective tensor might not be necessarily objective. For such a reason, specific objective derivatives have been constructed in order to remove parasitic rotations given by the strong anisotropy.

Hagege [130] has shown that the use of a classical objective derivation, such as Green-Naghdi and Jaumann, does not guarantee the objectivity of the behavior law. Indeed, the directions of anisotropy do not precisely follow the landmarks related to these derivatives, which rotate according to average rotations of the material.

Badel et al. [38] proposed to split the strain tensor into uncoupled deviatoric and spherical parts expressing longitudinal and transverse deformations. They asserted that under transverse compaction the material becomes stiffer in both spherical and deviatoric behaviors due to the high packing density. They added that with a pre-tension the compaction is stiffer. Nevertheless, the influence of longitudinal tension on the deviatoric behavior was neglected due to its arduous quantification. Moreover, to keep the yarn bending stiffness low, the longitudinal shear moduli are significantly lower than the longitudinal Young's modulus.

In both hypo- and hyper-elastic laws, the material coefficients of the yarn constitutive tensor need to be identified from different experimental tests. For example, the hypo-elastic law formulated by Badel et al. [38] required the identification of 4 parameters, whereas the hyper-elastic law developed by Charmetant et al. [80] law required the identification of 8 parameters (4 for elongation, 2 for compaction, 1 for distorsion and 1 for longitudinal shear strain energy), in their simple linear regime. While longitudinal Young modulus could be determined directly from a tension test on a single yarn, the identification of the transverse behavior is performed on a glass fiber plain weave fabric through an equibiaxial tension and pure shear tests attempting to significantly squeeze the yarns.

It is important to note that the number of coefficients to identify will depend on the basic assumptions the authors make (*e.g.*, orthotropic or isotropic behavior, deformation modes required) in addition to the basic hypo- or hyper-elastic laws. Hence, a direct comparison between both approaches cannot be done without taking into account these basic assumptions made by the authors. Moreover, they are useful in limiting the exponential inflation of constitutive parameters.

3.4. Micromechanical models

The **virtual fibers** in interaction have been used for the construction of micromechanical models due to the ease it provides. In a general sense, this astute modeling attempts at capturing the large deformation of

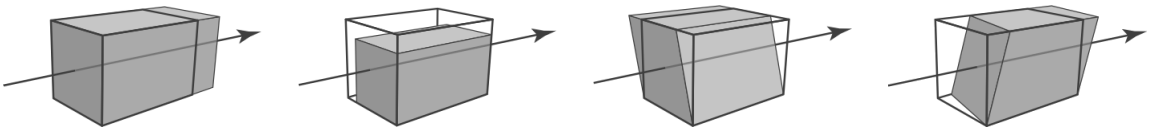

(a) (b) (c) (d)

Figure 8: Deformation modes of the yarn proposed by Charmetant et al. [80]: (a) elongation, (b) compaction of the cross section, (c) distortion of the cross section and (d) longitudinal shear; the arrow indicates the direction of fiber

the yarn cross section through the relative motion of the virtual fibers with a very small number of degrees of freedom. Indeed, many yarn features, such as cross section deformations and bending stiffness, can be captured using a limited number of virtual fibers instead of the thousands of real ones (*e.g.*, 25 virtual fibers can describe a yarn composed of 48k carbon fibers [18]).

The required constitutive parameters are those of the elementary fibers (considered as made out of an isotropic linear elastic solid) and their frictional properties. This very low number of parameters, whose value are *a priori* known or at least easily accessible, is the major strength of this approach.

This sub-mesoscale approach requires careful consideration of the many contact-friction interactions [18, 52, 131] between virtual fibers. This interaction limits their relative displacement within the yarn and effectively determines the highest intra-yarn fiber volume factor that can be achieved. Clearly such strategy, guarantees that yarn inter-penetrations are completely avoided. It is to be noted that this is one of the most severe limitations of geometrical approaches.

Moreover, this sub-mesoscale approach gives access to sub-mesoscale information that can be exploited at the mesoscale. For example, the mean yarn orientation can be obtained by integrating the orientation of the virtual fibers along the yarn path. Similarly, intra-yarn fiber volume fraction can be computed by analyzing the arrangement and cross section of the virtual fibers within the yarn cross section (the latter needs to be identified). Indeed, the modeling complexity introduced by the intra-yarn fiber volume fraction not being constant through the yarn can be readily captured by the virtual fibers although more subtle properties require more and more numerous fibers.

3.4.1. Virtual fiber concept

From a practical standpoint, to perform a simulation using virtual fibers, it is important to determine (i) their geometry, (ii) their initial arrangement, (iii) the number of virtual fibers that will be used, (iv) their mechanical properties, and (v) that of their interactions.

The number of virtual fibers used for representing a yarn is a trade-off between model fidelity (*e.g.*, complex yarn cross sections) and numerical complexity. Clearly, an increased number of virtual fibers per yarn, will better capture the yarn features and better approximate the overall yarn mechanical behavior. However, it will limit the number of yarns per unit cell that can be reasonably computed. As such, for a given simulation, there exists a "sufficient" number of virtual fibers that attains the desired complexity while providing results in a reasonable time frame. This issue has been explored by Green et al. [52] and Daelemans et al. [45] by comparing their simulations to X-ray tomography images of real fabric. While Daelemans et al. focused on a small number of virtual fibers (7, 19 and 37), Green et al. explored higher values (19, 37, 61 and 91). While the results from both authors differ, the chosen number of virtual fibers for the former is 19 and for the latter is 61, in both cases the choice was made by comparing the improvements on the overall yarn deformation (cross section shapes) with respect to the computational time and stability. For example, in the worst case a 50% increase of virtual fibers lead to a 140% increase in computational time. The authors propose, as a rule-of-thumb, that the number of virtual fibers should be chosen so as to guarantee that at least two or three virtual fibers be present across the thickness in the minimum dimension when the yarn is in its deformed state. Zhou et al. [84] performed a similar analysis and concluded that in most cases 19 to 50 virtual fibers might be sufficient to represent the yarn cross section geometry.

Next, the matter of virtual fibers disposition at the initial state has been explored by many. Frequently

used initial arrangement patterns are concentric circular [39, 44], elliptical [131] and hexagonal compact [18, 67] around the tow central line. It should be noted that, while this notion is nonexistent for the case of real fibers, it has been observed that it does play an important role in numerical simulations. For example, the choice of an hexagonal compact pattern (or a more globally dense one) numerically increases the intra-yarn fiber volume fraction, ideally up to a limit of approximately 91%. Although, Green et al. [11] observed that, for a real yarn, a value higher than 70-75% is impossible to reach since the fibers might be slightly misaligned or subjected to mutual entanglement. This high packing density could lead to dilatancy (under shearing) as well as strongly decreasing the mean free path (or distance between contacts) of fibers. The combination of these effects could considerably increase the yarn rigidity for bending and transverse compaction. Then, the main issue should not reside in numerically solving the problems that result from models with higher packing, but rather in limiting them to realistic packing levels. For example, Moustacas et al. [92] proposed to introduce a random internal sinusoidal perturbation of the virtual fiber paths. Thus, an initial intra-yarn fiber volume fraction lower than the one given by the standard hexagonal compact form can be achieved. While the addition of disorder in virtual fibers distribution attempts to reach a real yarn trend, its sinusoidal form does not allow to highlight the differential movement of virtual fibers in the cross section. Moreover, a (yarn) twisting step can also be considered during the initialization of virtual fibers [17, 18, 64, 91, 92] in order to maintain the internal yarn cohesion.

Next, with regards to the fiber geometry, Durville et al. [18] employed a simple relationship for defining the virtual fibers radii:

$$NR^2 = nr^2$$

where N is the number of virtual fibers chosen to describe the yarn, n is the number of (real) fibers within the yarn, r the radius of these fibers and R the radius of the virtual fibers. This kind of "natural" equivalence is widely spread as initial configuration [44, 52, 67, 87]. This relationship ensures a starting constant intra-yarn fiber volume fraction regardless of the virtual fibers radii and an identical extensional stiffness, with the same constituting material properties. However, bending stiffness may not always be properly scaled through this equivalence.

3.4.2. Virtual fiber models

Two approaches have been found in the literature: the digital element method [83] and the beam model [85, 86].

The **digital element method** proposed by Wang and Sun [83] discretizes the yarn into pin-connected (ball joint) digital rod elements. As such, a yarn is considered as a flexible 1D component with a (constant) circular cross section with the yarn flexibility being conveyed by frictionless pin connections. The authors estimate that the length of the digital elements needs to be relatively small (around half the radius of the virtual fiber) for conferring realistic yarn flexibility. Next, Zhou et al. [84] extend on the concept by modeling the yarn as a bundle of digital element chains, hence it is called the multi-chain digital element model. Both approaches (using one or multiple virtual fibers) were successfully employed for simulating the weaving and forming processes of 3D preforms.

The **beam model** proposed by Durville [85, 86] models the virtual fiber as a collection of beams. A finite strain beam formulation is employed in order to capture large deformations and admit contact-friction interactions. The stress–strain relationship for the beam model is based on a standard 3D constitutive law, such as the isotropic Saint Venant–Kirchhoff model, and leans on the virtual work principle for determining the static mechanical equilibrium. This virtual fiber formulation includes an enriched kinematics of the yarn cross section deformation. It approximates the affine transformation between the beam in an idealized state (constant circular cross section) and the beam in the deformed state (deformed cross sections) using a first order Taylor expansion. This approach was successful in simulating the unit cell of an angle interlock reinforcement containing 64 yarns, each of which was made of 25 virtual fibers [18] (1600 virtual fibers in total). Then, Moustacas et al. [73, 132] extended the initial enriched kinematics using a higher order Taylor expansion and implemented a decoupling of kinematic orders for the strain Green-Lagrange tensor calculation and also for the internal virtual work. This allows to set different behavior constitutive law (*e.g.*, transverse isotropic Neo-Hookean) according to the kinematic order. Such method allows fine tuning

the deformations involved in a given loading case. For example, this extension was successful in simulating transversal compaction of a yarn using only one kinematically enriched beam. However, although this mesomechanical approach allows greater transverse deformations of the cross sections, the process of setting different mechanical behaviors according to the kinematic orders emphasizes the question of the choice of the constitutive laws to fit the yarn behavior. It is of interest to emphasize that such an evolution can be compared with the mesoscale surrogate model: the number virtual fibers is now decreased to one, getting rid of the difficulty related to the computation of all frictional contacts, but at the expense of introducing a phenomenological constitutive law for the cross section, and an *ad hoc* parametrization of its shape.

Very recently, Daelemans et al. [87] proposed **hybrid virtual fibers** by overlaying the truss elements with beam elements. The idea is that the truss elements will determine the properties in the fiber direction such as the tensile stiffness, while the beam elements will confer the bending stiffness. The second moment of inertia is adapting by changing either the Young's modulus or the beam element radius.

It is noteworthy that the digital and the beam models follow opposite trends. While Zhou et al. [84] extends the approach of Wang and Sun [83] from one to multiple virtual fibers, Moustacas et al. [73] do the opposite with the approach of Durville [85]. On the one hand, the digital element method embraces the sub-mesoscale approach as demonstrated by the virtual fibers not increasing in complexity. On the other hand, the beam model migrates towards a mesoscale one by enriching the virtual fiber formulation and eventually decreasing the number of employed virtual fibers. Both strategies reflect on the freedom provided by this approach. Finally, hybrid virtual fibers have emerged by superposing digital and beam models [87].

3.4.3. Fiber interaction models

The problem of fiber interactions, due to its highly "non-smooth" mechanical character, calls for sophisticated treatments. The determination of contact surfaces, or the determination of their sticking or slipping character are by consequence very lengthy operations. As such, it imposes a limit on the number of virtual fibers that can be reasonably simulated (in a given reasonable time frame).

In the methods considered, two interaction conditions are commonly used for the virtual fibers: sticking and sliding. Here, the interaction force is composed of a normal component that accounts for the effects of pure contact and a tangential one related to the friction effects. The normal direction in the contact zones is orthogonal to the surfaces of the virtual fibers (their normal vectors can be shown to be necessarily collinear and opposite).

In order to simulate contact-friction interaction between virtual fibers, Wang and Sun [83] introduced contact elements between any two nodes when the distance between them is shorter than the virtual fiber diameter. These contact elements can support compression in the direction of the contact line and friction in the directions orthogonal to it (along the contact surface). Finally, an incremental method is used to simulate the contact process. The advantage of this approach is that contact is probed only from a discrete set of predefined points (the center of the rod elements). However, its drawback is that very accurate determination of the yarn surface normal and tangent vectors as well as the magnitude of the compressive forces are not attained. Hence, the effective coefficient of friction is not exactly the one introduced at each elementary contact. So an "artificial friction" (determined by the lateral component of the calculated compressive force) is set to prevent relative sliding motion between digital chains even when the friction coefficient is assumed to be zero. The authors suggest that to avoid this "artificial friction" the digital element length have to be inferior than 1/4 of its diameter.

Subsequently, Miao et al. [39] improved the previous the contact-interaction algorithm by introducing two modifications: the calculations of the contact element length (*i.e.*, distance between virtual fibers) and of the direction of compressive contact force between two digital chains (assumed to be perpendicular to digital chain). Indeed, the new algorithm is based upon a node-to-element distance rather than a node-to-node distance.

Durville [131] propose a method based on the determination of pairs of material particles predicted to enter into contact. This process follows the following stages: (i) determine the pairs of discrete contact elements by finding regions where contact is likely to occur (*i.e.*, proximity zones), (ii) compute an intermediate geometry for each zone as the average between the two parts of yarn path close to each other, and

(iii) choose a pair of particles candidates to contact on each of the surfaces amongst all points of this intermediate geometry. In this context, Moustacas et al. [73] improved the contact formulation by describing the intermediate geometry as a two-dimensional shape required by the yarn deformations offered by the enriched kinematics. This supplementary numerical sophistication provides a much more realistic contact geometry at the expense of a higher computation cost.

3.4.4. Towards the mesoscale

Once a desired textile configuration has been obtained (*e.g.*, a target overall fiber volume fraction or a target compaction level), the yarns are reconstructed from the virtual fibers that compose them. This reconstruction operation is a common practice since it does help in alleviating subsequent simulations (*e.g.*, less contact interactions to compute). In a general sense, the conversion from virtual fibers to yarns consists in: (i) computing the yarn path and cross sections, and (ii) obtaining the yarn surface.

Clearly, the first step requires a more sophisticated solution than the second one. It usually consists in first estimating the yarn path from the geometric center of the virtual fibers [51]. This path is then discretized by placing planes orthogonal to it at predefined intervals. Cross sections of the yarn need to be computed from the intersection of the virtual fibers with those planes. Placing them orthogonal to the yarn path avoids getting skewed cross sections in high crimp cases. The yarn path can then be updated by joining the centers of the newly obtained cross sections.

While the task of computing the yarn cross section may appear at first sight as a simple problem, it is quite arduous. First of all, the problem is a conceptual one since the yarn cross section is a useful geometrical abstraction that results from the arrangement of fibers. As such, it can be defined as the smallest region that encompasses all of the fibers within the yarn [106]. This problem is conceptually similar to that of finding the convex hull (also called convex envelope) of a set of points. This operation can be seen as stretching a rubber band around the subset of outer-most points [51]. However, as figure 9 shows, a convex shape may not suffice for properly capturing the cross section. This can lead to an overestimation of yarn area and cause significant inter-penetrations [133], especially for high compaction values (*i.e.*, very thin yarns).

For such reasons, Green et al. [11, 133] used the (locally-)modified version of the convex hull algorithm proposed by Gofman (see figure 9). They apply the method to the virtual fibers by only considering their center points (*i.e.*, no cross section). Then, consider an expansion of the found polygon by the radius of the elements in a direction perpendicular to the tangent of the polygon. This modified algorithm is driven by two parameters: (i) the number of neighbors taken into account when calculating the local average distance, and (ii) the search radius for the next candidate as proportional to the inter-fiber average distance. As such, any new point in the cross section will lie within the allowed search radius of the previous one and will creates a new line segment with the smallest external angle from the previous line segment, thereby defining a polygonal cross section. Let us to underline that in case of an infinite search radius, the simple convex hull is recovered and all points in the set become possible candidates. This additional control over the convex hull algorithm allows adjusting the desired level of smoothness of the cross section. However, it does not guarantee that consecutive cross sections will employ the same number of points. Hence, the authors employ a cubic interpolation function so as to provide a smooth transition between cross sections and generate a volume which can then be meshed.

A similar approach is followed by Said et al. [51] who developed a method that consists in shrinking an initial polygon (with a fixed number of points) down to the limits defined by the (outer) points. This approach, unlike the previous one, fixes the discretization of the yarn cross section. Such feature is useful for computing the yarn envelope, since the points in consecutive cross sections can simply be connected.

Alternatively, some authors [18, 44] have employed a variation of the ball-pivoting algorithm [135]. Here, the underlying concept is relatively simple: a circle of a given radius pivots from one sample point to another one, connecting them through edges. Clearly, according to the radius of the pivoting ball and the curvature of the outline, some points may not be reached by the pivoting ball.

It should be noted that, while this reconstruction step is the last one in the sub-mesoscale modeling chain, it deserves just as much consideration as the others. Indeed, given the considerable amount of effort and resources already devoted to obtaining a satisfactory arrangement of virtual fibers, it would be counterproductive not to do so. Moreover, this reconstruction operation must balance accuracy and

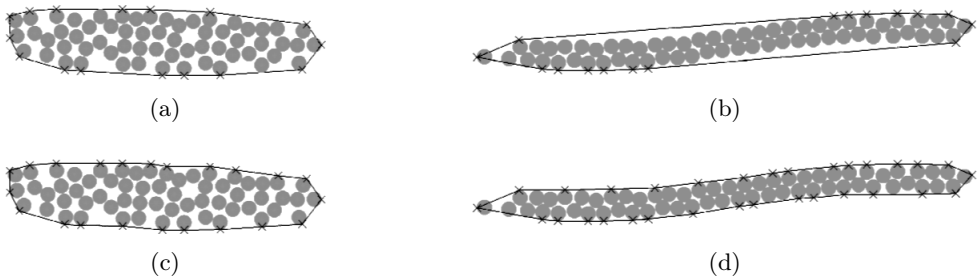

Figure 9: Example from Green et al. [133] that illustrates the application of (a)-(b) the classical convex hull and (c)-(d) the modified convex hull applied to two different yarn cross sections

complexity of the final yarn model (*e.g.*, properly describing a yarn cross section using the least amount of points).

Finally, these methods tend to overlook the fact that the new entities may no longer satisfy the same equilibrium conditions as their elementary virtual ones. Indeed, in terms of mechanical behavior, a dual-scale approach would better capture the kinematics of the complete textile. However, as the present calculations are mostly employed as initialization for subsequent ones, these differences should remain negligible.

3.5. Summary

As described in the previous sections, the numerical approaches devoted to yarn modeling are definitely various, creative and clever. This demonstrates the complexity to predict the yarn shape as well as to describe its deformation (*i.e.*, mechanical behavior). Table 1 summarizes the different modeling methods used in the literature.

Part of the complexity related to this task stems from the fact that the yarn is a collection of fibers. Indeed, their large number, their various orientations (twist factor, number of plies), make them very difficult to describe in spite of their individual simplicity (rigid cross-section, Coulomb solid friction) which require very few parameters. Indeed, this difficulty can be traced back to the great contrast between fiber properties (*e.g.*, between longitudinal and transverse elastic modulii) or geometrical properties (*e.g.*, between radius and length) which set this kind of problem as a non-smooth mechanics one. Moreover, the local arrangement of fibers can also play an important role in endowing the yarn with locally varying properties.

In this sense, **surrogate models** such as **geometrical modeling** propose an attractive alternative. Indeed, via purely geometrical means they attempt to capture the observed yarn variability instead of modeling the complex yarn behavior. In some cases, this representation can be simplified so as to depict an idealized version of the yarn (*e.g.*, constant circular cross section). In other cases however, these models can be enriched with *e.g.*, interpolating functions so as to capture the evolution of yarn cross sections along the yarn path, or surface-tension terms to smooth their boundary.

While purely geometrical models are limited in their representation capabilities (*e.g.*, capturing the "real" evolution of the yarn shape), they do provide a very good mesoscale initialization for **mesomechanical models**. These simulate the yarn under external mechanical loadings, hence require behavior laws to be defined. The most common ones have employed hyper- and hypo-elasticity frameworks. These two do capture the overall yarn behavior accurately, however they are limited in two aspects: (i) capturing the large yarn deformation at very low energies (at the beginning of the weaving) and (ii) capturing plastic deformations during the life of the yarn.

Micromechanical models emerge as a compromise between the simpler geometrical models and the complex mechanical ones. Sub-mesoscale models group bundles of fibers into the so-called "virtual fibers" as an alternative to the unaccessible modeling all the real fibers. Even though virtual fibers still require mechanical laws to describe their response, these are much simpler than the ones used in meso mechanical modeling (*i.e.*, hyper- and hypo-elastic laws). However, they involve intra-yarn contact interactions that need to be computed (*i.e.*, heavy computational cost). The number of virtual fibers per yarn used in the literature is summarized in table 2.

Table 1: Segmentation of yarn modeling references by model type and publication year

Model type	1997-2005	2006-2013	2014-2021	Total
Hollow shell		[16, 118]		2
Hyper-elastic	[79, 120]	[80, 122, 136]	[31, 137, 138]	8
Hypo-elastic	[129, 130, 139]	[38, 140]	[123, 141, 142]	8
Digital/truss element	[83, 84]	[39, 44]	[45, 50, 57, 64, 143, 144]	10
Beam element	[48, 85, 86]	[17, 67, 131]	[11, 18, 51, 52, 73, 76, 92]	13
Hybrid element			[87]	1

It is important to note that, because of their sound micromechanical basis, virtual fiber models have the potential to bridge the scales up to the textile (*e.g.*, transverse compaction test on a 5-layer angle-interlock textile [18]). This is also true for mesoscale approaches, but at the expense of having to calibrate the constitutive parameters of the yarns, often available only at the textile scale. Indeed, while the tensile behavior can be easily determined at the yarn scale, other deformation modes require ingenious experimental devices to do so. In addition to the yarn behavior, special attention should be paid to the inter-yarn interaction (contact and friction).

Both sub-mesoscale and mesoscale approaches have the potential to provide an accurate representation of the yarn behavior. The fidelity of this representation is dependent on factors such as the number of the considered degrees of freedom or the quality of the identification procedures for the constitutive laws. Using the beam model as an example, similar results for capturing the nonlinearities of a compaction test have been obtained at the sub-mesoscale [92] with 169 virtual fibers and at the mesoscale [73] with only one virtual fiber per yarn but with a third order enriched kinematics (which in turn requires many parameters). As such, the choice between a sub-mesoscale or mesoscale modeling approach is dependent on the desired yarn features to be captured (*e.g.*, geometrical shape, mechanical behavior). Indeed one can make the analogy between the number of virtual fibers employed for a sub-mesoscale approach and the number of degrees of freedom of a behavior law used at the mesoscale. As a rule-of-thumb, it has been shown that few dozens of virtual fibers are needed to approximate a continuum (*e.g.*, according to different authors, from 19 [45] to 91 [87]).

It is important to highlight that, for the case of virtual fibers and mechanical modeling, the choice of an initialization scheme is very important. For example, most sub-mesoscale approaches initialize virtual fibers with an hexagonal arrangement and most mesoscale approaches shrink the initial yarn cross sections so as to avoid interpenetations. While these strategies are useful, they often lead to unrealistically high initial intra-yarn fiber volume fractions. In this sense, solutions such as initial perturbations [92] or yarn inflation [16] can guarantee that a more realistic intra-yarn fiber volume fraction is achieved. On the contrary, the model should not be initialized with an intra-yarn fiber volume fraction too small because it could then be difficult to reach the desired final value. Overall, in order to accurately capture the evolution of the yarn shape under external loadings and to avoid spurious corrective methods, it is rather advised to initialize the yarn shape and volume as close as possible to reality.

As a final note, no literature has been found on the relationship between intra-yarn fiber volume fraction and yarn twisting. A consequence of this seemingly trivial connection is that while the intra-yarn fiber volume fraction for twisted yarns will not vary much when subjected to external loads, it will do so for untwisted yarns or yarns with low twist count. Indeed the internal cohesion in the twisted yarns will allow less relative motion of the fibers that compose it.

Table 2: Number of virtual fibers per yarn used in the literature

Nb.	2001-2007	2008-2014	2015-2021	Total
1-7	[83, 86]	[44]	[45, 144]	5
16-30	[17]	[39, 44, 52, 67]	[18, 45, 64, 144]	9
32-55	[39, 52, 84, 131]		[45, 64, 144]	7
61-91		[39, 44, 50, 51, 52]	[76, 87, 143, 144]	9
275-1183			[143]	1

4. Predictive approaches

For around two decades, Textile Generating Pre-Processors (TGP), such as **WiseTex** and **TexGen**, have been widely developed with the goal of numerically describing textile reinforcements (woven, braided and knitted) at the mesoscale with as few parameters as possible. They are "simple" geometry-based algorithms with idealized yarn paths and cross sections all along the principal direction. Similarly, Textile Generation Softwares (TGS) have also been developed with the goal of predicting realistic geometries by incorporating the mechanical behavior of the textile constituents. In many cases, TGP models can be used as initialization for TGS simulations.

The inherent challenge in predictive textile modeling is to accurately (realistically) describe the textile topology as well as the yarn morphology (*i.e.*, yarn path and cross sections), in particular at contact points between yarns. Indeed, an accurate representation of yarn path is crucial since waviness plays a significant role in the mechanical properties of the textile. Similarly, the many yarn cross sections (different along the yarn path) determine the local intra-yarn fiber volume fraction and thus its response to transverse compression, bending and traction.

All models start with the nominal textile topology (*i.e.*, weaving pattern) and, by means of a constitutive law that describes the yarn mechanical behavior, evolve from an "initial state" to an "as-woven" one. The latter tries to attain the configuration of the textile right after being woven and before any further processing (*e.g.*, forming). Furthermore, the employed constitutive law may provide either a very realistic and accurate description of the yarn mechanical properties, or opt for a more empirical and simpler geometry-based one. In particular, the differentiating factor between the two main types of predictive modeling is the ambition of modeling the weaving process or not. Indeed, reaching the as-woven state without taking into account the detailed history of the weaving process (*e.g.*, neglecting self-balanced internal residual stress field) requires many clever numerical shortcuts.

Once the (stress-free) "as-woven" state has been obtained, the next step is to simulate the forming process so as to reach an "as-manufactured" state. This final step consists in bringing the textile to a target shape, along with a target overall fiber volume fraction. In other words, the as-woven geometry serves as starting point for the as-manufactured simulation, hence it is a necessary step for describing the forming process.

Finally, the advantages of obtaining a realistic mesoscale description of the composite are many. For example, such model can be exploited for predicting the mechanical properties of the final part (*e.g.*, stiffness, vibration modes, damage). Similarly, it can be used to analyze and optimize either the weaving or forming processes, or even the textile architecture parameters. The ability to perform these calculations numerically, without requiring many expensive manufacturing iterations (*i.e.*, trial-and-error), is the key to performance enhancement, with the bonus of cost-effective improvements.

4.1. Simulating the weaving process

At mesoscale, the simulation of the weaving process requires a suitable mechanical behavior law and a finite deformation framework that properly accounts for geometrical non-linearities. In both cases, mathematical rigor and numerical efficiency and robustness are paramount. Despite the ambition of this task, many authors have tried to simulate the weaving process with different approaches allowing for a more or

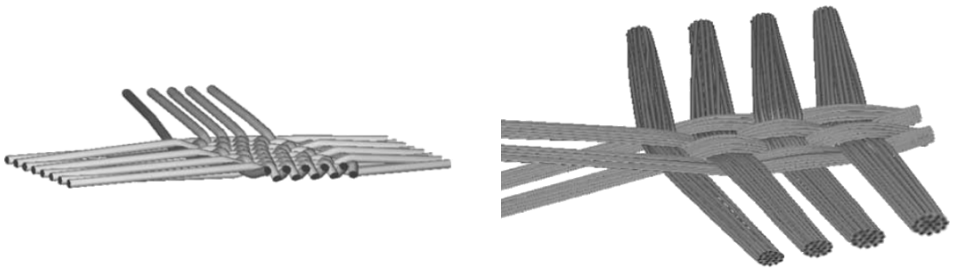

(a) (b)

Figure 10: Results for Zhou et al. [84], simulation of the 2D weaving the process using (a) single and (b) multi digital-chain element methods

less faithful woven geometrical description. In fact, this approach has already been explored for the case of 2D textiles [84] and 3D braids [83] using the digital element approach (see section 3.4.2), and has only very recently been done so for 3D woven composites [64]. Before detailing these recent works on 3D woven, it may be useful to recall the principles that guided the 2D woven and 3D braided (even if they are out of the scope of this paper).

First, Wang and Sun [83] simulated the 3D braiding process using one virtual fiber (digital chain) per yarn. They neglected yarn stretch since its elongation was assumed to be too small to affect the micro-deformations. Therefore, the stiffness of all the digital elements was replaced by a penalty factor with a large positive value. Besides, the authors used the stiffness perturbation method to avoid singular global stiffness matrix (*e.g.*, when any two neighboring digital-rod elements are aligned along the same straight line). Finally, positive yarn tension was applied to ensure the stability during the braiding process.

Then, Zhou et al. [84] extended the braiding process simulation to the 2D weaving process by employing either one or multiple virtual fibers per yarn (see figure 10). Here, inter-fiber slippage is also taken into account with inter-fiber solid friction interaction. Moreover, they assume that the yarn has a smooth surface with a zero-friction coefficient. These conditions allow to capture both yarn motion and cross section deformation.

Finally, Yang et al. [64] performed an impressive sub-mesoscale weaving simulation of a 3D through-the-thickness orthogonal interlock. They also employed the digital chain method (19, 30 and 55 virtual fibers per yarn) and an Abaqus explicit solver with linear elastic assumption for the yarn behavior. Additionally, the twist process is also simulated using Abaqus with a friction coefficient of 0.3 (measurements performed on quartz fibers [143]). They aim for 55 twists per meter on 3-ply warp, 10-ply weft, and 1-ply binder yarns. During the weaving simulation, tensions of 0.75 N and 0.25 N (measurements made by [145]) were applied to the moving ends of warp and binder yarns respectively. In each weaving cycle, the beating-up motions are simulated by moving the weft yarns along the warp and binder direction. Finally, transverse compression simulation is performed in order to reach around 43% of fiber volume fraction. These steps are shown in figure 11 along with a comparison of the obtained model with an observed sample. It can be seen that very realistic results are achieved by this approach.

4.2. Using surrogate modeling

Since the "as-woven" configuration is *a priori* unknown without a complete simulation of the weaving process (as in the previous section), the type of works that employ surrogate modeling do so by creating a starting configuration from which any further state (*e.g.*, as-woven, as-manufactured) can be achieved by simulation. In many cases, a "loose-weave" geometry is chosen, such that it respects the topology but with much separated yarns so as to avoid initial yarn interpenetration. Here, the well-known TGP can be used to get a nominal idealized geometry with these features. Additionally, most works enrich this initial geometry with measured textile characteristics (*e.g.*, yarn spacing) so that it can get as close as possible to the target one.

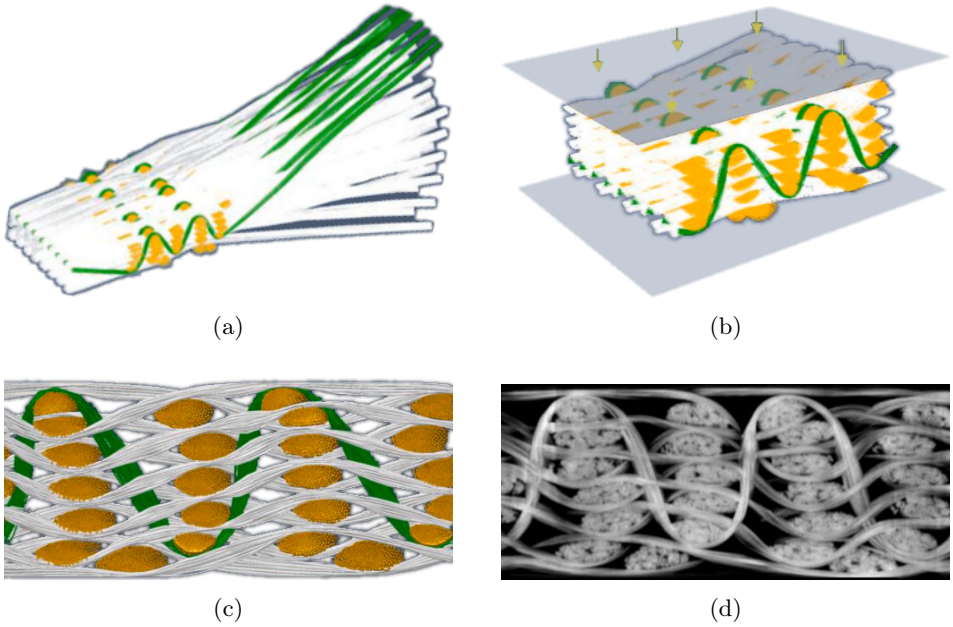

Figure 11: Results for Yang et al. [64], sub-mesoscale simulations of (a) the 3D weaving and (b) compression processes, and comparison between (c) sub-mesoscale model and (d) tomographic image

4.2.1. Textile and yarn features

The most essential parameter for properly describing a textile architecture is the weaving pattern. This parameter defines the type of reinforcement as well as providing a collection of "instructions" that define the relative positioning of yarns within a unit cell. By construction, it also determines some other topological parameters, such as the number of layers per column. Then, in order to fully define a textile reinforcement other geometrical parameters, such as yarn column spacing, are needed. Additionally, further information about the yarns needs to be provided (*e.g.*, number of plies, twisting amount, linear density).

Another important parameter is the textile thickness. This geometrical feature, along with others of more numerical nature (*e.g.*, dimensions of the Representative Elementary Volume), establish other textile characteristics such as the overall fiber volume fraction or the out-of-plane crimp. Experimentally, the thickness can be measured by compressing a fabric between two plates with a relatively small force [17] (Kawabata Evaluation System). Nowadays, X-ray tomography is mainly used for this task [52] since it can provide a more precise quantification of the fiber volume fraction as well as the out-of-plane crimp. This latter quantity is defined as the ratio between the curvilinear length and the end-to-end length [68].

Following this reasoning, one could argue that measuring some textile parameters can be seen as path for improving the prediction capabilities of numerical models, albeit at the cost of manufacturing samples and devising measuring methods. For example, Lin et al. [42] inspected samples using optical microscopy (LM) and scanning electron microscopy (SEM) for extracting more realistic measurements of the yarn cross sections. Similarly, depending on the chosen simulation strategy, other non-textile parameters (*i.e.*, mechanical parameters) may be required.

Finally, some recent efforts have been deployed to reduce as much as possible the number of parameters necessary to describe an as-woven architecture. Xu et al. [46] found that thirteen parameters are enough for completely defining the topology and geometry for a wide range of 2D and 3D weave architectures: five for the topology, and eight for the geometry (one of which is introduced for a convenient meshing procedure while the others are conventionally employed in modeling of textile composites).

4.2.2. Textile Geometry Pre-Processor (TGP)

For the last two decades, WiseTex [48] and TexGen [17] have been the TGP of choice for many wishing to model realistic 2D and 3D textile architectures. These have also been called meso-level textile processor (MLTP) [146].

WiseTex is a TGP which originates from KU Leuven (Belgium) and has been developed by Lomov et al. [14, 48, 147] capable of generating 2D and 3D fabrics with a minimum number of textile and yarn parameters. It defines the weaving pattern using a matrix coding method which describes the relative position of yarns. Then, the textile parametrization includes the weaving pattern and the inter-yarn distance. Next, the yarn properties that need to be defined are: yarn cross section type, yarn cross section dimensions (both in the free state), linear yarn densities, coefficient of friction between yarns. Currently, WiseTex supports cross sections of either circular, elliptical, lenticular, or rectangular shape. Usually, the shape in the free state is assumed to be circular or elliptic and the diameter is related to a few factors [14, 147]: the linear yarn density, the fiber density, its twist factor, and the intra-yarn fiber packing. Moreover, although these cross sections are fixed to be constant along the yarn path in the free state, they can vary in the relaxed state.

Undoubtedly, the most difficult parameters to define are the yarn bending and compression stiffness. Indeed, both play significant roles in the determination of the fabric micro-geometry, such as cross section shape and fabric thickness.

Internally, WiseTex subdivides both weft and warp yarns into "intervals of crimp" that represent segments of yarn between two consecutive intersections (figure 12). The shape of the yarn in this interval is computed using the principle of minimum of bending energy [148]. The idea is that for a given relative crimp height (crimp height over distance between the interval ends spacing), the yarn path, defined on a 2D plane, is computed by minimizing the bending energy. The latter is proportional to the experimental bending rigidity of the yarn, which depend on the curvature, and to the *characteristic function* of the crimp interval. Moreover, while bending and torsion behaviors are first assumed linear with constant rigidities [14], the bending rigidity is then set to depend non-lineary on the local curvature [148]. Then, the final relaxed yarn shape on the interval can be deduced from the computed transversal forces acting on it as yarn dimensions (in the direction and normal to the compressive force) have been measured experimentally in a compression test. Sometimes, a flat middle surface for each layer is enforced for the sake of convergence [40].

Finally, WiseTex also provides as output of the simulation the mechanical properties of the yarns. It allows extracting the local fiber packing within the yarn, the cross-sectional dimensions as well as the yarn curvature. For the micro to mesoscale transition, a Mori-Tanaka model is used for micro-homogenization [48] and also determining the stiffness tensor of the composite [66] during the meso to macroscale transition.

TexGen is an open source TGP developed at the University of Nottingham by Sherburn [17] and based on former works from Robitaille et al. [101, 149, 150]. The textile parameters it accepts are the weaving pattern, the number of warp and weft columns and layers, and the column spacing. Concerning the yarn cross section, depending on the targeted fabric it admits circular, elliptical, power ellipse, lenticular, race-track, polygon or hybrid shapes [106]. The latter is useful for reducing yarn inter-penetration as it allows to set any combination of the ellipse, power ellipse, lenticular sections to a selected sector of the cross section. Some yarn properties can also be defined: yarn linear density, fiber density, fiber diameter, number of fibers per yarn and the elastic properties of the fiber. These are currently used in the calculation of the fiber volume fraction as well as within the export functions to calculate the yarn or composite properties. Note that, TexGen does not require the bending rigidity to be defined.

Recently, **UnitCells** was developed by Li et al. [53] as an *add-on* to Abaqus based on TexGen and HyperMesh. This tool, also developed at the University of Nottingham, allows leveraging the strengths of each of these softwares (simulation, textile geometry, meshing) so as to get a complete composite material characterization tool.

DMFA (Digital Fabric Mechanics Analyzer) is an open source software developed at Kansas State University based on works of Wang and Sun [83] and Zhou et al. [84]. Consequently, it implements the digital element method detailed in section 3.4.2. It should be noted that DFMA is itself also a TGS since it uses a main solver for performing the TGP function, for performing simulation of the weaving process

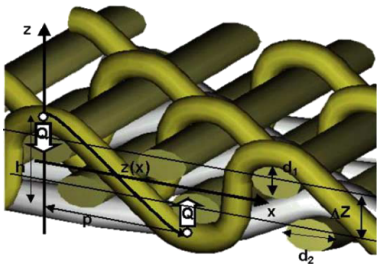

Figure 12: Representation of the mesoscale woven structure from WiseTex on a crimp interval proposed by Verpoest and Lomov [148]

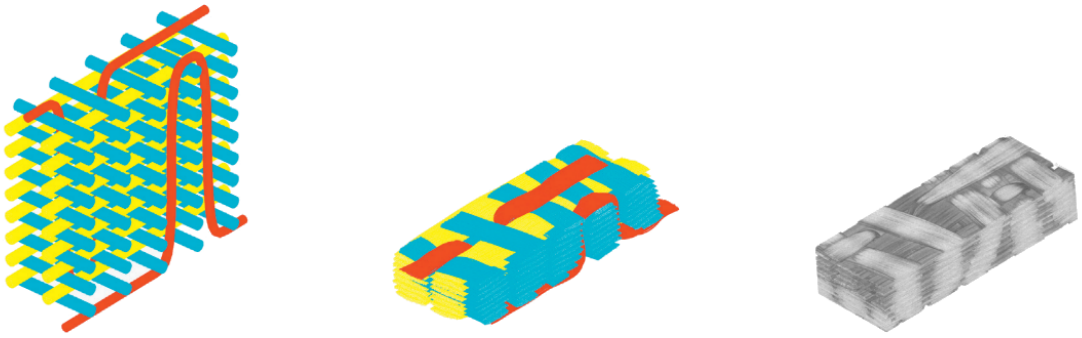

(a) Loose-weave model (b) As-manufactured model (c) CT scan

Figure 13: Results from Green et al. [52] for simulation of an orthogonal through-the-thickness interlock

for 2D woven and 3D braided fabrics, as well as for performing fabric stress, strength deformation, impact, molding and draping analyses.

Finally, some recent works have found alternatives to the previously listed TGP. For example, Daelemans et al. [45] developed an in-house Python script, while Mahadik and Hallett [67] and Dewangan and Panigrahi [63] employed the FE softwares MSC Patran and Digimat [151], respectively. Just like with UnitCells, these approaches that employ FE solvers offer complete solutions that integrate the preparation, simulation and post-processing (*e.g.*, Digimat also integrates a mean-field homogenization of yarns).

4.2.3. Towards the "as-woven" state

Mahadik and Hallett [67] use a beam element formulation and an in-house TGP script (using MSC Patran) for obtaining the initial idealized geometry. This initial configuration is converted into a FE mesh that depicts the loose-woven state (see figure 13a). Next, loading of yarns is simulated to generate an as-woven fabric. This deformation is modeled as a step-by-step process of applying tension forces to the yarns, subdividing them into more virtual fibers and relaxing the unbalanced stresses. Here a temperature drop is applied on the binder yarns causing them to contract and hence apply compaction forces to the fabric until a desired thickness is achieved. This strategy follows the previously discussed analogy with thermo-elasticity to tune the eigen strain. Finally, to reach the "as-manufactured" configuration, transverse compaction is performed with rigid plates until the target thickness is reached.

Green et al. [52] improve the method proposed by Mahadik and Hallett [67] through their use of TexGen as TGP, see figure 13b. Then, Said et al. [51] profit from the flexible geometric description provided by TexGen to also describe the final as-manufactured textile at the mesoscale, see figure 14. And, Daelemans et al. [45] adapt the method to the digital element method since, unlike the beam element formulation, truss element-based virtual fibers have no bending stiffness (hence no need to artificially reduce it). Also, Daelemans et al. [45] use Abaqus for all FE simulations, unlike previous authors that use LS-DYNA.

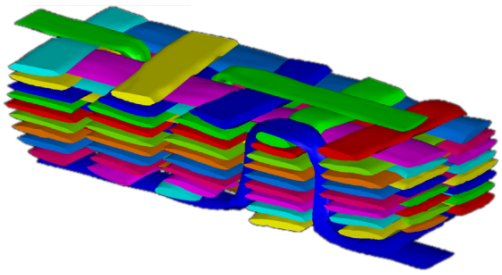

Figure 14: Results of the mesoscale reconstruction from Said et al. [51] for an orthogonal through-the-thickness interlock

Miao et al. [39] propose a static relaxation approach based on the (multi-chain) digital element method [84]. This method is an alternative to the very expensive step-by-step process of textile simulation [83, 84]. Indeed, it achieves a reduction of 90% of the computational cost by modifying the contact-interaction algorithm (section 3.4.3) and neglecting the effects of yarn-to-yarn and chain-to-chain friction on micro-geometries. The proposed approach starts with an initial configuration provided either by using a TGP or by a simple simulation of the textile process using only one virtual fiber per yarn (*i.e.*, DFMA). Then, this mesoscale description of the textile is converted into a sub-mesoscale one by subdividing each yarn into multiple virtual fibers. Afterwards, a pre-tensile-strain (or stress) is applied to each virtual fiber in order to imitate the tension effect that produces a tight fabric structure. This produces unbalanced forces at nodes. Upon relaxation, the fabric reaches a new equilibrium state (*i.e.*, the as-woven state).

Huang et al. [44] and Drach et al. [50] propose fiber-level dynamic relaxation procedure using periodic boundary conditions and a (virtual) dynamical framework to attain a balanced rest configuration. Just as Miao et al. [39] do, they employ DFMA as a TGP for obtaining an initial configuration using only one virtual fiber per yarn, and then subdividing each yarn into multiple virtual fibers and re-discretizing each virtual fiber at each simulation step. However, unlike static simulations that require the global stiffness matrix be computed in each iteration [39], the dynamic relaxation process does not. This leads to a multi-level relaxation procedure that significantly reduces computing time. It should be noted that with this strategy the stiffness matrix is often either singular or ill-conditioned due to the virtual fiber flexibility. This results in slow convergence rate. Then, the proposed approach consists in increasing the number of virtual fibers at each relaxation step. With each simulation step in the dynamic relaxation loop including 4 sub-steps: (i) a predetermined tension is applied to yarns, (ii) the periodic boundary zone is established through a mapping process, (iii) contacts between fibers and nodes are determined, and (iv) nodal forces, accelerations, velocities, displacements as well as new nodal locations are computed within the unit cell. This relaxation process gradually dissipates the potential energy through an addition of a damping coefficient. The numerical simulation continues until the potential energy approaches a minimum state and the kinetic energy vanishes.

Very recently, Daelemans et al. [87] developed an overlay mesh technique by decoupling the in-plane and out-of-plane properties of the virtual fiber. They create hybrid virtual fibers with truss elements that determine the properties in the fiber direction (tensile stiffness), and beam elements that provide bending stiffness without affecting the properties along the fiber (*i.e.*, negligible Young's modulus). The proposed method uses DFMA as a TGP and Abaqus for the as-woven simulation using the same procedure as Green et al. [52]. Then, through-thickness compression (quasi-static explicit simulation) is performed for achieving the as-manufactured state. Note that the contact between the virtual fiber is imposed on the truss elements only and is defined by Abaqus General Contact algorithm. This method is a continuation of the works of Daelemans et al. [45].

Durville [85, 86] developed **MultiFil**, a quasi-static algorithm based on the modeling of a collection of elastic beams (*i.e.*, yarn beam model). Unlike previous methods, the initial configuration used here is not a loose-weave one, but a completely inter-penetrated one where all yarns have straight trajectories and are placed on the same plane (see figure 15a). Then, a contact-friction algorithm is used for progressively separating the yarns until the textile topology is restored (see figure 15). Here the topology is used to

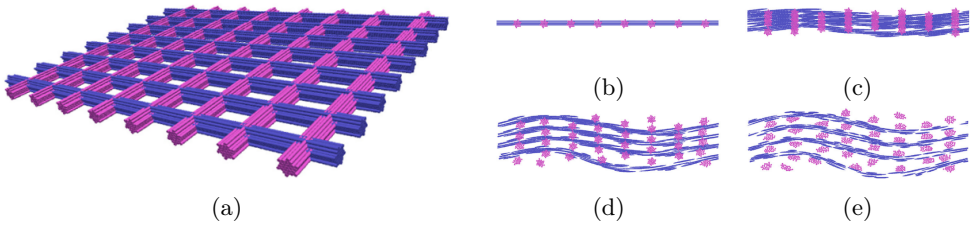

Figure 15: Results from Durville et al. [18] showing (a)–(b) the starting interpenetrated configuration, followed by (c)–(e) the separation steps

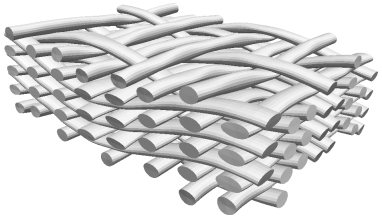

Figure 16: Results from Moustacas et al. [73] for an as-woven state of an angle layer-to-layer weave simulated at the mesoscale

manage the yarns displacement into the correct direction by setting the orientation of the contact surface. After all yarns are completely separated, the relaxation process of the entangled structure is performed. It consists in solving for the displacement field of all virtual fibers via a weak formulation based on the virtual work principle. Here, the internal virtual work is formulated in a (finite transformation) Lagrangian setting where (hyper-)elasticity of the virtual fibers, contact and friction between them and boundary conditions can be exploited. Recently, the works of Moustacas et al. [73, 132] on the enriched beam kinematics have been implemented in MultiFil. Thus, making it one of the few TGS that can inherently simulate both at the sub-meso and mesoscale (see figure 16).

4.3. Summary

As it can be seen in table 3, a clear distinction can be made between Textile Geometry Pre-Processors (TGP) and Textile Generation Softwares (TGS). Here, the determining factor are their respective input and outputs. Among all cited softwares, both WiseTex and DFMA are complete modeling suites that integrate both TGP and TGS. As such, not only can they provide an initial idealized geometry, but they also perform simulations to attain the as-woven and as-manufactured states. Table 4 displays the use of the different TGP and TGS through the years.

Most works employ the well established TGP and TGS tools (*e.g.*, WiseTex, TexGen, DFMA, MultiFil) for obtaining the as-woven configuration. They have the advantage of requiring considerably less parameters than the alternative (simulation of the weaving process). Thus, they demand a relatively lower computational effort. For doing so, they employ some ingenious modeling strategies, capable of correctly describing the reinforcement and capturing most of the mechanical and geometrical properties of the yarns. In this sense a correct evaluation of these parameters has proven to be very important.

Instead, Yang et al. [64] opt for a less explored route and show that a complete simulation of the 3D weaving process is possible. Obviously, this presents some major caveats such as requiring elevated computing resources or the need for more parameters. Indeed, the authors did not give many details on some implementation aspects nor on the definition of some key parameters. Future improvements on this technique could consider further mechanical states that the yarns experience during the weaving process, such as initial pre-tension, inter-yarn friction during beating-up motions or natural relaxation.

Table 3: Summary of predictive methods (surrogate modeling only), the different input and output configurations are shown in *italics* and the software types representing their relative steps are shown in **bold**

<table>
<tr><td colspan="6">Feeding parameters</td></tr>
<tr><td rowspan="2">TGP</td><td>In-house scripts
Daelemans et al. [45]</td><td></td><td>TexGen
Sherburn [17]</td><td rowspan="3">WiseTex
Lomov et al. [48]</td><td rowspan="3">DFMA
Wang and Sun [83]
Zhou et al. [84]</td></tr>
<tr><td colspan="3">Idealized geometry</td></tr>
<tr><td>TGS</td><td></td><td>MultiFil
Durville [86]</td><td>UnitCells
Li et al. [53]</td></tr>
<tr><td colspan="6">As woven / as manufactured</td></tr>
</table>

Table 4: Segmentation of the literature on predictive approaches by publication year

Softwares	1997-2005	2006-2013	2014-2021	Total
WiseTex	[14, 48, 109, 147, 148]	[26, 49, 66, 114, 152]	[31, 40, 146]	11
TexGen		[16, 17, 42, 106, 118]	[5, 11, 12, 51, 52, 53, 56, 60, 153]	14
DFMA	[83, 84]	[39]	[44, 45, 50, 57, 87]	8
MultiFil	[85, 86]	[131]	[18, 73, 92]	6
UnitCells			[46, 53]	2

It is interesting to note that, from most of the literature, sub-mesoscale modeling is considered as more attractive than the more difficult mesoscale approaches. Indeed, the abstraction provided by the virtual fibers allows for strategies such as progressive refinement (*i.e.*, adding more and more virtual fibers to their yarns [44]) and capture more accurately the non-homogeneous geometry of the as-woven yarns. This strategy has proven satisfactory for studies using TexGen and DFMA as TGP. In this sense, the recent developments of MultiFil made possible the use of the same beam model formulation for either a sub-meso or mesoscale modeling, just by increasing the number of degrees of freedom for the beam cross section.

Similarly, while most works seek an initial configuration that depicts the textile in a yarn interpenetration-free state, MultiFil [18, 86, 131] does the opposite. Indeed, these works start with an initial configuration that is not physically admissible in which yarns are inter-penetrated. Then, a progressive separation driven by a sophisticated contact-friction algorithm is performed to remove the yarn inter-penetration of the "fully compacted" configuration. As such, it avoids resorting fictitious tensioning operations such as those used by Green et al. [52], Said et al. [51] and Daelemans et al. [45] (*i.e.*, contraction of yarns).

Finally, it is noteworthy that the "ubiquity" of many predictive softwares has led developers to integrate their simulation capabilities into most of the fully-fledged softwares. That is the case of DFMA, used both with Abaqus or LS-DYNA, and UnitCells, that extends TexGen features by taking advantage of Abaqus and HyperMesh. On the contrary, WiseTex provides a fully integrated package along with its "brothers" VoxTex (in imagery) and FlowTex (in permeability analyses). This all-encompassing strategy allows complete analysis pipelines on most of the aspects of 3D woven textiles, but also hinders its applicability in other FE contexts.

5. Descriptive approaches

This collection of methods relies on images, more precisely volume images (or 3D images) of real samples. These images are obtained using high-resolution X-ray computed tomography (μ-CT), a method of choice that gives access to the inner structure of the material in a nondestructive fashion. As such, the goal of descriptive modeling is to extract usable textile models from these images. These textile models usually take the form of either geometrical descriptors (see section 3.2.1) or Finite Element (FE) meshes. For both

cases, image processing and statistical analysis techniques are required for reliably extracting the required information. Poor contrast, image noise and standard tomographic artefacts are common challenges that need to be addressed.

It is important to note that, unlike the case of 2D composites, research on 3D woven composites is still actively being developed. Nonetheless, some innovative methods have been proposed by building upon the experience on 2D weaves.

Indeed, two distinct types of approaches have been identified in the literature. The first type of methods aim at obtaining voxel-masks for each of the segmented entities. These are then converted into usable models (*e.g.*, FE meshes) and usually require an intermediate clean-up step (*e.g.*, removing spurious segmented voxels). The second type of methods integrates all steps into complete procedures. As such, unlike previous methods that optimize (*e.g.*, tune) each individual step individually, these methods do reach a global minimum (as defined by a loss function). Both of these strategies have shown to yield satisfactory results for different types of interlock composites at different image resolutions (from around 1μm [38, 54, 82] up to 25μm [38, 69, 154, 155, 156]).

5.1. Segmentation using voxel masks

This group of methods "transform" the image information (*i.e.*, gray level values) into feature information. This latter representation (often high-dimensional) provides different novel criteria that can be employed for separating the entities of interest. This is often performed using advanced statistical methods, such as clustering analysis.

The most common strategy for performing this "transformation" is based on the analysis of the preferential orientation of the local image texture [55, 157]. Clearly, the motivation behind this type of approaches stems from the highly oriented nature of the yarns that compose the textiles. Hence, it seems natural to exploit such information for identifying and further segmenting yarns. Next, a more abstract approach based on the texture of the components was proposed [54]. This demonstrates a move towards a more *abstract* conceptualization of the image characteristics. Such trend is even more clear in the novel deep learning applications [62, 75] wherein the feature information is autonomously learnt by the Convolutional Neural Networks (CNN). These CNN are capable of constructing complex models by assembling simpler patterns in the training data.

5.1.1. Using the structure tensor

The structure tensor [158] (also known as symmetry tensor, orientation tensor, inertia tensor or moment tensor) is a useful tool used to compute or represent local orientation fields. Its analytical extension to yield the *generalized structure tensor* [159] allows to detect more intricate patterns than straight lines and edges, hence propelling for its use as an unsupervised method for segmenting image textures [160]. For a given image H and its gradient $\boldsymbol{\nabla} H$, the structure tensor is defined as

$$S = K * (\boldsymbol{\nabla} H \otimes \boldsymbol{\nabla} H)$$

with K being either a simple normalized ($\iint K = 1$) integration window or a Gaussian kernel. As from its definition, S is a non-negative symmetric 3×3 matrix, that can be diagonalized, so that, at each voxel location, the principal orientations of anisotropy are obtained by the eigenvectors, denoting the (local) directions with the largest and the smallest changes in gray levels, while the magnitude of the change is associated to eigenvalues. A proper choice of K is fundamental for allowing an average integration comparable to yarn cross section, avoiding confusion of yarn orientation. As a consequence, the largest eigenvalue should surpass the level of noise in the image, hence it cannot be too small.

As seen in figure 17, for segmentation tasks, the structure tensor is used to differentiate between fully isotropic regions (*e.g.*, the pore space between yarns, where all eigenvalues are similar, represented here by spherical glyphs) and highly anisotropic ones (*e.g.*, the interlaced yarns, denoted by glyphs flattened along the fiber path, and elongated along the two transverse principal orientations to the yarn path). This simplicity and effectiveness in terms of accuracy has made it the preferred tool for segmenting tomographic images of woven textiles, both for 2D [82] or 3D weaves [55, 157, 161].

However this orientation information provided by the structure tensor by itself is, in most cases, impractical for a direct segmentation procedure. For such reason, it is usual to condense this information into some key features, such as the degree of anisotropy [55]. This latter, defined as the complement to 1 of the ratio between the smallest and the largest eigenvalue of the structure tensor, tends towards 0 for isotropic components (matrix, air) and 1 for anisotropic ones (yarns, fibrous plies). Similarly, it can also be augmented by other pertinent features, such as the local average gray value (within the same integration window) [55, 157, 161].

However, a "simple" threshold on either of these features will not provide the best results [55]. For example, ring artefacts may be confused with yarns, or, for the case of 3D textiles, the features associated to the binder yarns are neither very different nor similar to the weft and warp ones. Moreover, textiles with elevated compaction levels tend to present multiple yarns in contact (even at high resolution), making their separation non trivial. In such cases, a proper definition of the yarn contours becomes a complex task.

This leads to the natural choice of clustering analysis for classifying each voxel in the image, and relating it to a multi-dimensional vector collecting all these features (*e.g.*, eigenvalues, eigenvectors, average gray level, orientation vector, degree of anisotropy), naturally exploitable for multi-class classification algorithms.

Straumit et al. [55] employ an unsupervised clustering technique called ***k*-means** that aims to partition the data points into k clusters where each point belongs to the cluster with the nearest centroid. They carry two analyses on image features: the first one relates the local degree of anisotropy with the local average gray value, whilst the second employs the degree of anisotropy along with the warp component of the orientation vector. As reported in figure 18 they find that by employing this method, only few entities can be separated (for example, the second analysis separates the yarns of different orientations (*i.e.*, the weft from the warp), while the first one only the reinforcement from the matrix and air). Moreover, it has been shown that k-means clustering for segmenting woven textiles produces an underestimation of the solid volume fraction with respect to the volume of yarns [154].

Hence, Liu et al. [157] propose a supervised approach using a multi-variate **Gaussian Mixture Model** (GMM) pertaining to a three-component feature vector. This contains: (i) the average gray value, (ii) the degree of anisotropy, and (iii) the orientation vector in the form of an azimuthal angle. The algorithm optimizes a defined number of Gaussian distributions, each related to a material component (in this case three Gaussians representing the matrix, the warp and the weft), and seeks the optimal mean and variance of each distribution. The authors propose to initialize the Gaussians with some carefully chosen small 3D regions. The resulting segmentation (shown in figure 19) provides the complete separation of the three different materials (*i.e.*, yarns, resin and voids) and the subdivision of the yarns cluster. However, the algorithm has issues in cases of contacting yarns (*e.g.*, the warp and the binders) and gathers them into a unique group, noted "collective warps". Finally, due to the non-local nature of the approach, the yarns may require some clean-up as post-processing.

These previous methods (using k-means [55] and GMM [157]) have been implemented into the VoxTex software developed by the Composite Materials Group from the KU Leuven (Belgium). It is also important to note that a complete separation of weft, warp and binder yarns cannot be achieved only with these tools and require further processing (to be detailed in the next section) but they provide a very solid ground for segmentation.

5.1.2. Surrogate modeling of images

Naouar et al. [54] propose a novel approach based on texture analysis based on the well known Haralick texture features [162, 163]. These features characterize the pixels with respect to their intensity and spatial neighbors.

Obtaining these features is a three step process. First, the original image is quantized so as to obtain a reduced (discrete) number of gray levels. Second, the distribution of co-occurring gray level values at a given offset is computed using a sliding window for all pixels in the image. And third, useful statistics from the co-occurrence matrices are extracted, these are the Haralick features. This allows obtaining a vector of features for each pixel in the original image.

In the study of Naouar et al. [54], the authors analyze different Haralick features and empirically retain only one. Effectively, they obtain another image (of the same size as the original) with the gray values

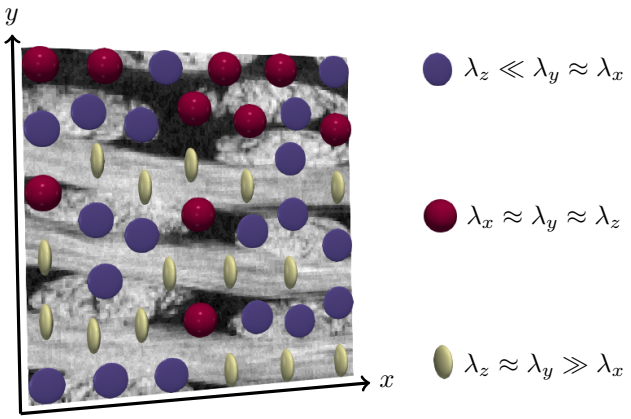

Figure 17: Visualization of an *ideal* application of the structure tensor on a µ-CT image (a slice shown here) with the principal orientations depicted by the corresponding glyphs. Note that the anisotropic glyphs are similar to flat disks with normals aligned with the yarn orientation.

(a) (b) (c)

Figure 18: Segmentation results for Straumit et al. [55] (a) µ-CT image, (b) k-means clustering by the anisotropy and average gray value, (c) k-means clustering by the degree of anisotropy and warp component of the orientation vector

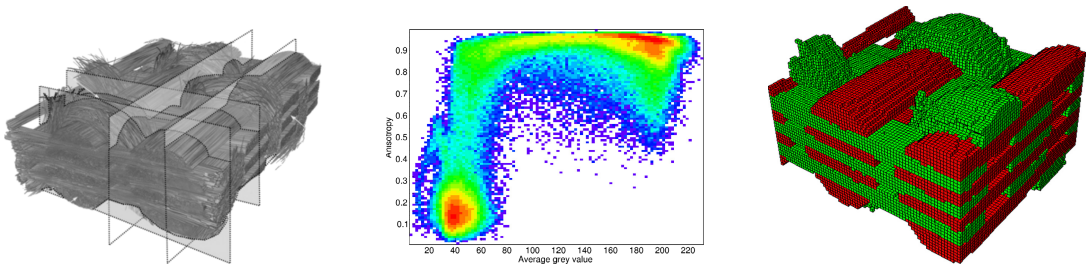

(a) (b) (c)

Figure 19: Segmentation results for Liu et al. [157], the segmented unit cell with matrix hidden (a) µ-CT image, (b) constructed feature space, (c) results using GMM

(a) (b) (c)

Figure 20: Segmentation results for Naouar et al. [54] (a) chosen textural feature, (b) segmentation by thresholding, (c) final results by morphological operations

representing the relative texture differences instead of the X-ray attenuation. The studied material is a through-the-thickness orthogonal interlock. Then, a simple thresholding followed by some standard morphological operations (dilation, erosion) lead to the final segmentation. The results are shown in figure 20.

5.1.3. Deep learning applications

Ali et al. [62, 164] propose to employ DeepLab v3+ [165], a state-of-the-art CNN in *semantic segmentation* with encoder and decoder modules (in this context, semantic segmentation is identical to plain segmentation). The encoder module produces multi-scale high level feature representations (see figure 21a) thanks to a residual network ResNet18 [166] pre-trained on more than a million images from the ImageNet dataset [167]. Next, the decoder module refines the segmentation results along object boundaries by accessing an intermediate representation of the same ResNet18 and combining it with the feature map from the encoder module. The authors employ a 2D strategy for the segmentation (*i.e.*, independently feed slices of the stack to the network), albeit they use a less than common top-down approach (*i.e.*, the slices are taken in the thickness direction). The slices are then manually annotated using the MATLAB Image Labeler Tool. They perform this operation for a 2D plain woven glass fabric and a 3D orthogonal woven carbon fabric, hence constructing two training datasets. These are then used to train two different networks, the results are shown in figure 21b. By comparing the segmentation results to the ground truth, the authors note that the performance for the binder yarns is lesser than that for the warp and weft yarns. This is to be expected, since the orthogonal binder yarns are barely visible in the chosen slicing view (parallel to the textile plane).

It should be noted that the authors also construct two more "virtual" datasets (one for each type of fabric) and train two more networks. Clearly, the motivation for segmenting these virtual images (for which everything is perfectly known) is not to exploit the segmentation results but to "assess" the performance of the network. However, it could be argued that such evaluation is highly dependent of the chosen method for constructing these virtual images and not inherent to the neural architecture.

Recently, Blusseau et al. [75] proposed two approaches for semantic segmentation using a U-Net [168] architecture. The first approach consists in predicting the yarn center lines by analyzing 2D slices of a 3D volume. This requires the yarn paths to be annotated so that the center points are know for any given slice. These are encoded as binary masks in which the pixels closest to any center point are valued 1 and all other are valued 0. As expected, the output of this approach requires heavy post-processing for identifying the actual center points from the predicted score maps. The second approach aims at predicting the signed distance function for each yarn cross section. This approach should be more robust than the first one since it is a generalization of the former. However, given that the only given information are the manually annotated yarn paths, they employ a sequence of fine-tuned morphological operations to construct some annotations. It should be noted that, while this pseudo-labeling may not be perfect, it is much easier to obtain than doing it manually and should provide enough information for the networks to learn the yarn signature. Finally, both methods are tested on two 3D woven composites with different compaction levels. They explore different configurations: training different networks on each sample (independently), on each yarn orientation, or combining both samples. The best results are obtained for the first approach when training on both samples (compacted and un-compacted) but only on the warp orientation.

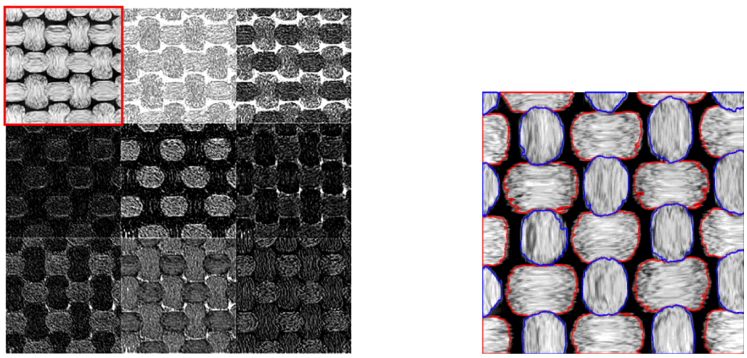

(a) (b)

Figure 21: Results from Ali et al. [62] using a CNN, (a) some of the automatically learnt features (*i.e.*, descriptors), and (b) results on a 2D fabric

5.2. Obtaining usable textile models

In the previous section, all methods output voxel-wise binary masks for each identified instance. Hence, unless a voxel-based formalism is employed [10], they do necessitate further processing in order to provide usable textile models (*e.g.*, FE meshes).

Moreover, given that these approaches perform the segmentation on a "feature-space", they cannot guarantee spatial consistency. For such reasons, they often require some post-processing "clean-up" steps before and after the construction of the textile models. These are performed using tools as simple as morphological operations [54] or as unusual as the cellular automata [55].

It is important to recall that the previous methods are only capable of distinguishing between yarn orientations (*e.g.*, weft, warp, binder) but not of isolating each yarn. For cases in which the yarns are not heavily compacted, simple morphological operations can be employed (*e.g.*, connected components) [54]. However, in more complex cases, such as two yarns of the same type being in contact, some manual intervention may be necessary [169].

Most meshing strategies require these last two steps of clean-up and yarn isolation as mandatory preprocessing. However a novel pipeline that encompasses all these steps as been proposed [161, 170]. These two radically different strategies will be detailed in the following.

5.2.1. Meshing-only strategies

Naouar et al. [54] proposes an expansion algorithm for meshing each cross section. First a rough approximation of the cross section is obtained by overlapping a grid of contiguous equilateral triangles and selecting only those fully included within (see figure 22a). This mesh is then expanded using a linear elastic formulation until the section boundaries are reached (see figure 22b). Finally, only the boundary nodes are kept and a Delaunay triangulation is used for meshing the surface (see figure 22c). This last step helps in avoiding badly conditioned meshes. Finally, the independently optimized meshes for two consecutive cross sections are joined together using prismatic (wedge) elements. A final resulting mesh is shown in figure 22.

Huang et al. [59] use a dual kriging interpolation method for estimating parametric surfaces from series of selected representative slices. This step however creates yarn interpenetration that is dealt with using a voxel formalism. As such, the voxel description of the yarns is first contracted so as to guarantee no intersections. Then, each yarn is dilated iteratively until it reaches the original border or another yarn. Finally, a parametric model is fitted again on these voxel representations. Given that the authors chose to use the same formalism as in TexGen, they are limited in the variety of cross sections and are forced to keep a uniform shape for each yarn type (*e.g.*, lenticular, power ellipse).

It should be noted that the motivation behind this complicated procedure (from parametric to voxel descriptions and back to a parametric one) is not clear. Moreover, the end result (using the TexGen formalism) looses much of the precision achieved at previous steps.

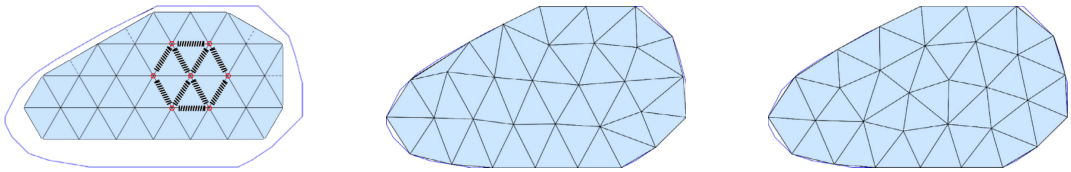

(a) (b) (c)

Figure 22: Meshing strategy for yarn cross sections proposed by Naouar et al. [54], (a) initial grid-like configuration, (b) after linear expansion, and (c) after Delaunay triangulation. Note that only the boundary nodes are kept in the last step

Ewert et al. [169] extract the section boundaries (edge detection) and use the remaining point coordinates for fitting basis splines on it. These are then used to construct NURBS surfaces by interpolating between the fitted splines. Next, these parametric surfaces are imported into a meshing software so as to fill the yarns using tetrahedral elements. Importantly, in order to be able to properly mesh the matrix too, the authors take care of separating the yarn surfaces (by contracting them) so as to guarantee gaps between any contacting yarns. Finally, the remaining empty space is meshed to generate the matrix volume. The results for a unit cell volume are shown in figure 24b, where the volume results from two mirror operations since only a quarter of the unit cell was meshed.

It should be noted that, only Naouar et al. [54] is constructing the textile model starting from automatically obtained results (see previous section). Indeed, the works of Huang et al. [59] and Ewert et al. [169] are based on manual segmentation of the images using either custom or readily available software (*e.g.*, ImageJ). However, in principle, these methods could be used in conjunction with any of those that provide binary masks (*e.g.*, those using the structure tensor or deep learning).

5.2.2. Integrated modeling pipeline

Wintiba et al. [161] provide an integrated meshing method, capable of transforming the resulting voxel mask from VoxTex software [55, 157], into a full textile model in the form of a conformal FE mesh.

They propose to use the alpha shape [171] operation on the binary masks. The alpha shape is a generalization of the convex hull that consists in enveloping a cloud of points so as to describe its boundary. The MATLAB implementation of the alpha shape provides great versatility since it allows for interactive manipulation (*e.g.*, to tighten or loosen the fit around the points). Indeed, unlike the convex hull, the alpha shape is capable of extracting individual entities.

When applied to the binary masks, the alpha shape will provide (triangular) individual surfaces of the single yarns (*i.e.*, identification of yarn contours). For the case of the weft mask, no issues are found since there are no contacting weft yarns. Yet, for the case of "collective warps" mask (see previous section), the obtained surfaces merge at times the warp and binder yarns. In order to properly isolate these yarns, the local orientations are employed to identify the only horizontal structures (warp yarns) from the undulating ones that correspond to binder yarns. The alpha shape for the warp yarns is computed followed by the same operation on the remaining binder yarns. See figure 23 for the intermediate results of this step.

Given that the alpha shapes for each yarn orientation are computed independently, some yarn interpenetration remain. Here, the authors propose the use of a level set method for identifying the interface surface between contacting yarns. They estimate the signed distance function by dilation of the yarn surfaces in regular intervals. As such, they profit from the information readily available from the alpha shapes.

Finally, the transition from the level set geometry to a tetrahedral mesh is performed using a multi-step process [170]. First, the marching cubes algorithm is applied on the level set geometry to obtain a triangular mesh of the surfaces. While the resulting triangulation tends to present ill-shaped elements (*e.g.*, too small or narrow), they serve as a constraint for the tetrahedral mesh generation process. This latter is obtained by Delaunay triangulation. Again, this triangulation is not guaranteed to construct "high-quality" meshes, hence the resulting volume mesh is deformed so as to obtain a fictitious mechanical equilibrium in which

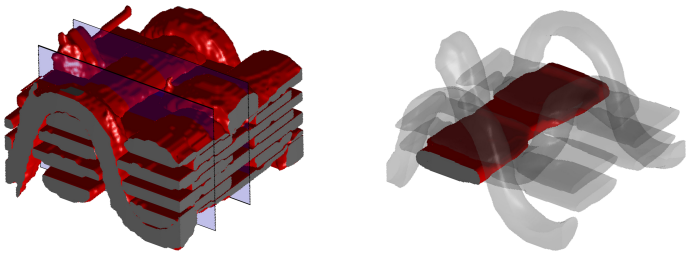

(a) (b)

Figure 23: Processing steps of Wintiba et al. [161] (a) alpha shapes describing the yarn surfaces, and (b) isolation of some yarns

(a) (b) (c)

Figure 24: Resulting FE meshes obtained by: (a) Naouar et al. [54], (b) Ewert et al. [169], (c) Wintiba et al. [161]

the element edges approximate to a desired average element length. The resulting high fidelity mesh is illustrated in figure 24c.

5.3. Segmentation using integrated methods

These integrated methods employ some previous knowledge about the textile being analyzed. While this does require some previous work to be performed, they have the advantage of being able to benefit from any information that is available from a previous analysis (*e.g.*, the yarn ID can be known beforehand from the textile model).

Here, the methods using geometrical priors start with a known textile definition and seek to optimize its parameters (*e.g.*, yarns cross sections). Given that the topology is known, these methods have the advantage of being extremely robust to cases in which two (or more) yarns are so heavily compressed against each other, that they become visually indistinguishable. Indeed, the final result will always produce the expected number of yarns.

A recent use of deep learning within an integrated pipeline has also been proposed. This presents a clear departure from the previous applications that would output voxel masks (*e.g.*, Ali et al. [62]), thus requiring post-processing for obtaining the textile model.

5.3.1. Geometrical priors

Bénézech and Couégnat [69] proposed a segmentation approach that employs a parametrized geometrical model that is iteratively improved using a heuristic optimization process. The employed parametrization follows the same principles as outlined in section 3 with the yarn cross sections being described using either ellipses or polygons. Importantly, the yarn paths are initialized by manually defining a reduced number of control points. Moreover, the optimization consists in minimizing an objective function that estimates the correctness of the geometrical model at a given state. This function is given as the weighted sum of three

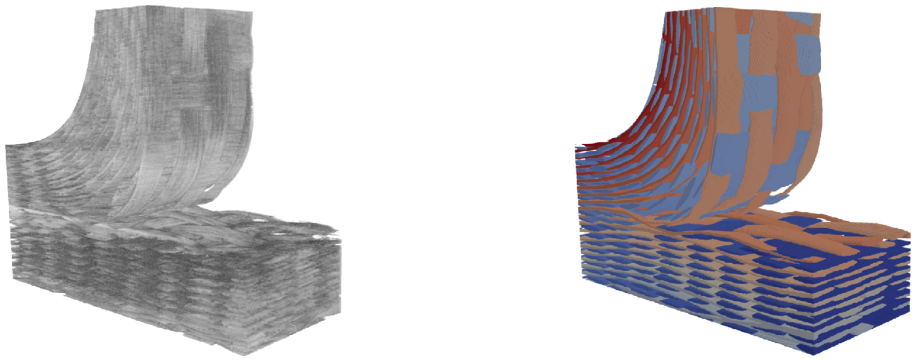

(a) (b)

Figure 25: Segmentation results from Bénézech and Couégnat [69] with geometrical prior on a CMC woven junction

terms, with the weighting terms being adapted during the global iterations of the algorithm. These terms are:

- A mask similarity metric that promotes the matching of the envelope of the geometrical model with the boundaries between matrix and reinforcement. This is obtained by computing the Jaccard index, also known as Intersection over Union (IoU), between the voxelized geometrical model and the binary mask of the textile.
- A constraints metric that promotes the consistency between the local directions of the yarns (from the structure tensor) and the direction of each segment of the geometrical model (from the local yarn path).
- A regularization metric that penalizes unrealistic yarn configurations (*e.g.*, aspect ratio of a cross section exceeding a given limit) and yarn interpenetration (from the voxelized geometrical model).

Given that the objective function is not guaranteed to be smooth nor convex, the authors propose a heuristic optimization scheme. This method, similar to a Monte-Carlo procedure, that consists in randomly permuting some of the geometrical parameters and evaluating if the similarity score increases or decreases. If the permutation is beneficial, it is kept, otherwise the parameters revert back to their previous values. For simplicity, the authors perform this operation on local subsets of the global model and optimize them simultaneously (while avoiding race conditions between consecutive subsets). Moreover, they propose to start with a "simplified" model using only elliptical cross sections (the yarn path is known from the initial manual operation). Then, after some iterations (*e.g.*, a third of the total) the elliptical cross sections are switched to polygonal ones.

The method was successfully applied on a couple of layer-to-layer interlock samples and a complex woven junction, see figure 25. The analysis of this $800 \times 800 \times 300$ voxel volume took around 30 hours on a 40-core CPU with a manual pre-processing of around 6 hours (identification of yarn paths). As the authors remark, while the computation time is considerable, the "effective" time of the manual identification of the yarn paths is mostly accessible and even more so considering the complexity of the analyzed volume.

Mendoza et al. [72] proposed a *correlation framework* in which a prior textile model is "deformed" so as to conform to a CT image. The method is based on a non-rigid image registration procedure between a voxelized version of the textile model and the CT image. It should be noted that, while the geometrical model employed here is based on elliptical cross sections, these are only "effective" once the final model has been obtained. As a matter of fact, the geometrical model is "smoothened" during the voxelization process so that the obtained gray levels indicate a function to the closest yarn path. This function is valued one at the yarn path and linearly decreases towards zero at the yarn envelope, it is also valued zero for all voxels not contained by any yarn.

The method employs a multi-scale registration process using Digital Volume Correlation [71]. The principle is to subsample both images (model and CT) and use the results from registration at the coarser

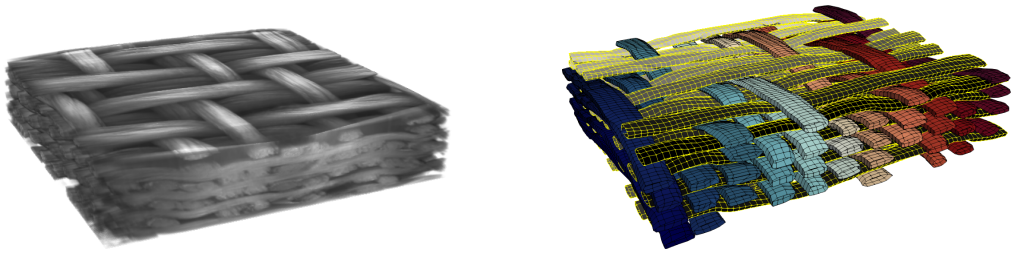

(a) (b)

Figure 26: Results from Mendoza et al. [74] using FE simulations and CNN, (a) original CT volume, and (b) obtained mesh

scale to initialize registration at the finer scale. Three additional scales (each time halving the resolution) are used for first globally aligning the textile and, as the finer scales are explored, locally adjusting the yarns. It should be noted that the "smooth" voxelization of the geometrical model allows the registration to be more tolerant on the inaccurate placement of the yarn boundaries and mainly focus on the yarn path. Therefore, after registration has converged, only the yarn paths are kept and elliptical cross section are attributed to all yarns. Moreover, if a more precise segmentation is desired for cross sections, this result could be used as initialization for methods such as the one proposed by Bénézech and Couégnat [69]. Finally, the method was applied on a pair of through-the-thickness angle interlock samples. Moreover, the method was able to cope with missing yarns and correctly placed the theoretical yarns (from the prior model) where these would be in the real textile.

5.3.2. Deep learning

Mendoza et al. [74] pose the problem of yarn segmentation as one "instance segmentation" via key points estimation. Typically, instance segmentation consists in performing object detection along with semantic segmentation. In this case, the semantic segmentation is replaced by key point estimation. Here the objective is two-fold: to detect yarns in a given image, and to describe each yarn using the respective key points. It should be noted the meshing procedure is trivial after a key point description of the yarns is obtained, as it can be as simple as connecting the key points to form either linear, surface or volume elements.

CNN have proven to be very effective for problems such as these (*e.g.*, human pose estimation). However, one of the biggest challenges with this type of approaches is the need for well-annotated data. In this case, as they analyze 2D slices of the 3D volume (in the warp and weft orientations), the dataset should consist on pairs of CT slices and lists of manually identified key points (for each yarn present in the image). In order to avoid this laborious process, the authors propose to use FE simulations to construct a synthetic database. However, while these may provide "perfectly" placed key points for every cross section, the images one would obtain from the voxelization of the deformed FE models do not bear any resemblance to real CT images. For such a reason, a U-Net architecture [168] is proposed for solving the *image translation* problem that would convert any simply labeled image (*e.g.*, simple voxelization of a textile model) into a realistic CT image. In order to do so, the yarn paths of a real CT volume are manually annotated and a simple textile model is constructed using elliptical shapes. The U-Net is then trained on slices from this pair of images (textile model as input and CT as output). After training of the U-Net, a 12-step compaction is performed on a numerical textile and these FE meshes are converted into realistic looking CT images.

Then, a Mask R-CNN architecture [172] is trained on these 12 new volumes. Here the network is given as input the "pseudo" CT images and is tasked with predicting the key points extracted from the FE meshes (10 points describing the yarn cross section contour and 1 center key point for the yarn path). Finally, after training, the Mask R-CNN model is used on a real sample and the results of connecting the key points is shown in figure 26. It is important to note that, even when the Mask R-CNN was trained on uniquely numerical data, the pseudo CT images produced by the U-Net are so realistic that it is capable of generalizing to real CT images.

5.4. Summary

A summary of the reviewed methods can be seen in table 5. Here, each approach is shown according to the position it holds in the processing chain. It can be seen that most methods approach the individual steps using different "building blocks" that can *almost* be freely assembled. This can be seen in the continuity between the works of Liu et al. [157] and Wintiba et al. [161], for example. Moreover, these could lead to novel procedures (*i.e.*, pipelines). For example, in principle, one should be able to combine the segmentation step of Liu et al. [157] with the cleaning methodology of Straumit et al. [55] and the meshing strategy of Naouar et al. [54].

Unfortunately, these methods only allow for the information to flow in a single direction. More precisely, once one step has been accomplished, it is never questioned again and the subsequent methods cannot benefit for any information that may have been available previously. A clear example is the complete procedure developed by Naouar et al. [54] (segmentation, cleaning, meshing) in which each step is performed completely independently from each other.

A novel class of methods emerges which aims at integrating the once individual collection of steps into a complete chain where each link can iteratively be refined so that a global consistency is achieved. For example, the technique proposed by Bénézech and Couégnat [69] aims at incorporating all these similar steps into a holistic optimization scheme. Then, all the uncertainties and errors made from each step are accounted for and optimized so as to minimize them altogether. The same can be said for the strategy employed by Wintiba et al. [161] since they encompass the process from binary masks up to textile models.

The same evolution could be observed in the manner in which the image information is analyzed. Indeed, the most natural approach of exploiting the highly oriented nature of the material lead to earlier methods based on the structure tensor [55, 157]. Then, a more pragmatic conception using deep neural networks [62, 74, 75] was proposed. These do not seek to identify or define physically relevant quantities but rather exploit and benefit from the tremendous progress of completely general and mostly agnostic methods stemming from deep learning. While currently these methods are only in their infancy (*i.e.*, using "off-the-shelf" CNN architectures), their efficiency could dramatically be enhanced as soon as a more specialized and tailored frameworks become available.

By combining these two trends, one could image descriptive modeling techniques of the future to be *end-to-end* (*i.e.*, integrated pipelines) and based on advanced learning or optimization methods. These approaches would avoid the seemingly necessary step of using binary mask and directly provide the necessary elements for constructing the textile models. Indeed the works of Wintiba et al. [161], Bénézech and Couégnat [69] and Mendoza et al. [72, 74] point towards this philosophy.

Finally, only the works of Straumit et al. [55] and Liu et al. [157] are currently accessible to the general public through the VoxTex software. Additionally, only the method proposed by Bénézech and Couégnat [69] shows to be capable of extracting the textile model of volumes bigger than the unit cell. The scalability options for the other approaches remains to be proven.

Table 5: Summary of descriptive methods in the literature, the different input and output elements are shown in **bold** and the individual steps are shown in *italics*

µ-CT	*Segmentation*	**Binary masks**	*Cleaning*	**Yarn contours**	*Meshing*	**Textile model**
					Dual kriging Huang et al. [59]	
					NURBS Ewert et al. [169]	
	Texture analysis Naouar et al. [54]		Morphological operators Naouar et al. [54]		Elastic expansion Naouar et al. [54]	
	k-means Straumit et al. [55]		Cellular automata Straumit et al. [55]			
	Deep Lab v3+ Ali et al. [62, 164]					
	U-Net Blusseau et al. [75]		Morphological operators Blusseau et al. [75]			
	GMM Liu et al. [157]		Alpha shape Wintiba et al. [161]			
	Deformable model Bénézech and Couégnat [69]					
	Registration method Mendoza et al. [72]					
	Mask R-CNN with U-Net Mendoza et al. [74]					

6. Conclusion

After this overall review of the wide and rich literature about the numerical modeling of woven composites, the diversity and cleverness of different approaches proposed to connect the theoretical design of a sophisticated engineered material with outstanding performance to its concrete manufacturing (in particular through tomographic observation) is astounding. The available variety of approaches is a vivid testimony of the creativity that has been deployed to address these questions.

The purpose of this review, and hence of its conclusion, is not to give figures of merit to these numerous works. Not only they have different qualities and limitations, but the fine-tuning of the trade-off between simplicity and sophistication is highly subjective. Moreover, they do not all focus on the very same goal and hence any ranking would be unfair. Nevertheless, a distant-view of this beautiful panorama, allows some general observations to be made, and trends to be identified.

Overall, two distinct strategies have emerged from the bibliography: the *predictive* and the *descriptive* approaches. While the former attempts to predict the as-woven and as-manufactured states of woven fabrics starting from yarn properties and textile design, the latter extracts the mesoscale geometry of actual preforms from µ-CT images. Predicting the actual structure of a fabric, or reading it from an image are both challenging.

Topology is important as it defines the woven structure, but it is clearly insufficient to be usable by itself. Geometry at first has to come into play, but also reveals to be limited. Then, mechanical modeling of yarns is a natural extension. Yet, some extreme cases of constitutive laws do capture geometry and not much more. For instance a constant density of fibers in yarn cross-sections can be seen either as a geometrical constraint (*e.g.*, cross-section area not being smaller than a prescribed threshold) or a mechanical one (divergence of the bulk modulus for a defined fiber volume fraction). In particular, mechanical modeling introduces such a constraint only as an asymptotic regime (allowing for some variations around this limit), and hence may reveal to be both, more flexible and more realistic.

However, this flexibility comes with a cost: dealing with the mechanics of yarns, a complicated topic on itself. On the one hand, mesoscale modeling treats the yarn as a single entity with phenomenological properties, thus requiring the identification of material parameters from experimental tests. On the other hand, sub-mesoscale modeling treats the yarn as a collection of virtual fibers that collectively mimic the yarn behavior with very few parameters, however it needs to deal with the issues related to non-smooth mechanics (*i.e.*, contact and friction). Both strategies have shown impressive results and have permitted gaining further insight on woven composites (beyond the scope of the present study) such as resin infiltration or mechanical properties of finished parts (stiffness, resistance to fracture, damage, or fatigue). It may be interesting to note that some aspects that are absolutely crucial from a technological point of view are seldom discussed in the literature (*e.g.*, the role of the fiber sizing, the presence of a controlled amount of water during weaving or forming, the twisting of yarns for weaving, etc.).

Clearly, tomography of real textile has the undeniable advantage of reality. Yet, being descriptive of a particular (physical) state, it lacks the ability to forecast how the textile would behave under future conditions. These questions can however be addressed by properly extracting the constituents in the image, and endowing them with the above discussed geometrical and mechanical properties. It should be noted that this "enrichment" of the yarn could serve as a useful regularization for the ill-posed problem of image segmentation. Moreover, by exploiting image registration (*e.g.*, between two samples), this model could be transferred to a comparable but different weave, hence allowing to transport any available relevant information (*e.g.*, properties, yarn label, FE mesh).

From the above considerations, it is obvious that descriptive and predictive are not opposed but complementary. It is only through their composition that a fair description of the textile may be reached. Here, the composition implies that no intrinsic hierarchy between the different tools is imposed *a priori*. Indeed, since they all bear some pieces of information, they should all be conceived for allowing information to flow in both directions (as either input or output). Moreover, the trustworthiness of the different quantities, be they mechanical or geometrical properties, may be questioned and possibly revisited so that they provide a better account of the observations, and finally providing a validated global overview.

As a final comment, the success of the recent artificial intelligence or machine learning approaches that

were mentioned in this review is astounding. This success is all the more fascinating considering that the mechanical modeling, just advocated to be the key to empowering the descriptive approach, is not explicitly taken into account. Hence, it may be tempting to envision a characterization of the woven composite as a comprehensive object, with its topology, geometry and mechanics should be treated as a whole regardless the approach (including machine learning). In this direction, the inclusion of topology preserving constraints in deep neural networks, for instance, has been shown to lead to more efficient and more reliable data interpretation. Constitutive law identification from data-driven approaches can also be seen as a recent and attractive trend. The association of these different tools, in a version more dedicated or specialized to fabrics, may constitute in the years to come, a formidable way to further progress in getting the best of these quite remarkable materials.

7. Acknowledgments

Marcello Rubino acknowledges the support of a PhD grant N°2019/1662 from ANRT and Safran Aircraft Engines. The authors would like to thank the anonymous reviewers for their careful reading and thoughtful comments.

References

[1] G. Marsh, Aero engines lose weight thanks to composites, Reinforced Plastics 56 (2012) 32–35.
[2] M. Patel, B. Pardhi, S. Chopara, M. Pal, Lightweight Composite Materials for Automotive - A Review, Concepts Journal of Applied Research 3 (2018) 1–9.
[3] T. Norton, T. Hassan, M. Mohamed, S. Rizkalla, Behavior of 3-D Woven Glass Fiber Reinforced Polymeric Bridge Deck Slabs, in: International Conference: Future Vision and Challenges for Urban Development, 2004, pp. 1–11.
[4] P. Bussetta, N. Correia, Numerical forming of continuous fibre reinforced composite material: A review, Composites Part A: Applied Science and Manufacturing 113 (2018) 12–31.
[5] S. Yan, X. Zeng, A. Long, Effect of fibre architecture on tensile pull-off behaviour of 3D woven composite T-joints, Composite Structures 242 (2020) 112194.
[6] W. Tao, Z. Liu, P. Zhu, C. Zhu, W. Chen, Multi-scale design of three dimensional woven composite automobile fender using modified particle swarm optimization algorithm, Composite Structures 181 (2017) 73–83.
[7] M. Umair, K. Shaker, M. U. Javaid, M. Kashif, Y. Nawab, M. Hussain, M. Kashif, Effect of weaving patterns on damage resistance of 3D woven jointless T and H shaped reinforcements, Mechanics of Advanced Materials and Structures 0 (2020) 1–14.
[8] J. Wang, P. Wang, N. Hamila, P. Boisse, Mesoscopic analyses of the draping of 3D woven composite reinforcements based on macroscopic simulations, Composite Structures (2020) 112602.
[9] J. Schneider, G. Hello, Z. Aboura, M. L. Benzeggagh, D. Marsal, A meso-FE voxel model of an interlock woven composite, in: ICCM International Conferences on Composite Materials, Dic, Edinburgh, Scotland, 2009, pp. 1–11.
[10] G. Hello, J. Schneider, Z. Aboura, Numerical Simulations of Woven Composite Materials With Voxel-FE Models, in: 16th European Conference on Composite Materials (ECCM 2014), June, 2014, pp. 22–26.
[11] S. D. Green, M. Y. Matveev, A. C. Long, D. Ivanov, S. R. Hallett, Mechanical modelling of 3D woven composites considering realistic unit cell geometry, Composite Structures 118 (2014) 284–293.
[12] B. El Said, F. Daghia, D. Ivanov, S. R. Hallett, An iterative multiscale modelling approach for nonlinear analysis of 3D composites, International Journal of Solids and Structures 132-133 (2018) 42–58.
[13] S. Mathieu, N. Hamila, F. Dupé, C. Descamps, P. Boisse, Stability of 3D Textile Composite Reinforcement Simulations: Solutions to Spurious Transverse Modes, Applied Composite Materials 23 (2016) 739–760.
[14] S. V. Lomov, G. Huymans, Y. Luo, R. S. Parnas, A. Prodromou, I. Verpoest, G. Huysmans, Y. Luo, R. S. Parnas, A. Prodromou, Textile composites : modelling strategies, Composites Part A: Applied Science and Manufacturing 32 (2001) 1379–1394.
[15] F. Desplentere, S. V. Lomov, D. L. Woerdeman, I. Verpoest, M. Wevers, A. Bogdanovich, Micro-CT characterization of variability in 3D textile architecture, Composites Science and Technology 65 (2005) 1920–1930.
[16] F. Stig, S. Hallström, Spatial modelling of 3D-woven textiles, Composite Structures 94 (2012) 1495–1502.
[17] M. Sherburn, Geometric and Mechanical Modelling of Textiles, Ph.D. thesis, University of Nottingham, 2007.
[18] D. Durville, I. Baydoun, H. Moustacas, G. Périé, Y. Wielhorski, Determining the initial configuration and characterizing the mechanical properties of 3D angle-interlock fabrics using finite element simulation, International Journal of Solids and Structures 154 (2018) 97–103.
[19] L. P. Djukic, I. Herszberg, W. R. Walsh, G. A. Schoeppner, B. G. Prusty, D. W. Kelly, B. Gangadhara Prusty, D. W. Kelly, Contrast enhancement in visualisation of woven composite tow architecture using a MicroCT scanner. Part 1: Fabric coating and resin additives, Composites Part A: Applied Science and Manufacturing 40 (2009) 553–565.

[20] L. P. Djukic, I. Herszberg, W. R. Walsh, G. A. Schoeppner, B. Gangadhara Prusty, B. G. Prusty, D. W. Kelly, Contrast enhancement in visualisation of woven composite tow architecture using a MicroCT scanner. Part 2: Tow and preform coatings, Composites Part A: Applied Science and Manufacturing 40 (2009) 1870–1879.
[21] M. Ansar, W. Xinwei, Z. Chouwei, Modeling strategies of 3D woven composites: A review, Composite Structures 93 (2011) 1947–1963.
[22] T. Gereke, C. Cherif, A review of numerical models for 3D woven composite reinforcements, Composite Structures 209 (2019) 60–66.
[23] N. Naouar, D. Vasiukov, C. H. Park, S. V. Lomov, P. Boisse, Meso-FE modelling of textile composites and X-ray tomography, 2020.
[24] A. P. Mouritz, M. K. Bannister, P. J. Falzon, K. H. Leong, Review of applications for advanced three-dimensional fibre textile composites, Composites Part A: Applied Science and Manufacturing 30 (1999) 1445–1461.
[25] R. Kamiya, B. A. Cheeseman, P. Popper, T.-W. Chou, Some recent advances in the fabrication and design of three-dimensional textile preforms: A review, Composites Science and Technology 60 (2000) 33–47.
[26] S. V. Lomov, A. E. Bogdanovich, D. S. Ivanov, D. Mungalov, M. Karahan, I. Verpoest, A comparative study of tensile properties of non-crimp 3D orthogonal weave and multi-layer plain weave E-glass composites. Part 1: Materials , methods and principal results, Composites Part A: Applied Science and Manufacturing 40 (2009) 1134–1143.
[27] M. N. Saleh, C. Soutis, Recent advancements in mechanical characterisation of 3D woven composites, Mechanics of Advanced Materials and Modern Processes 3 (2017).
[28] K. Bilisik, Multiaxis three-dimensional weaving for composites: A review, Textile Research Journal 82 (2012) 725–743.
[29] F. K. Ko, G. W. Du, Textile Preforming, Handbook of Composites (1998) 397–424.
[30] S. Mathieu, P. Boisse, N. Hamila, F. Bouillon, Locking and Stability of 3D Woven Composite Reinforcements, Key Engineering Materials 611-612 (2014) 292–299.
[31] J. Pazmino, S. Mathieu, V. Carvelli, P. Boisse, S. V. Lomov, Numerical modelling of forming of a non-crimp 3D orthogonal weave E-glass composite reinforcement, Composites Part A: Applied Science and Manufacturing 72 (2015) 207–218.
[32] S. G. Advani, E. M. Sozer, Liquid Molding of Thermoset Composites, in: Comprehensive Composite Materials, volume 2, Pergamon, 2000, pp. 807–844.
[33] P. Šimáček, S. G. Advani, Desirable features in mold filling simulations for liquid composite molding processes, Polymer Composites 25 (2004) 355–367.
[34] F. Trochu, E. Ruiz, V. Achim, S. Soukane, Advanced numerical simulation of liquid composite molding for process analysis and optimization, Composites Part A: Applied Science and Manufacturing 37 (2006) 890–902.
[35] I. Y. Chang, J. K. Lees, Recent Development in Thermoplastic Composites: A Review of Matrix Systems and Processing Methods, Journal of Thermoplastic Composite Materials 1 (1988) 277–296.
[36] K. K. Chawla, Ceramic matrix composites, Springer Science & Business Media, 2013.
[37] S. Z. Sheng, S. Van Hoa, Modeling of 3D angle interlock woven fabric composites, Journal of Thermoplastic Composite Materials 16 (2003) 45–58.
[38] P. Badel, E. Vidal-Sallé, E. Maire, P. Boisse, Simulation and tomography analysis of textile composite reinforcement deformation at the mesoscopic scale, Composites Science and Technology 68 (2008) 2433–2440.
[39] Y. Miao, E. Zhou, Y. Wang, B. A. Cheeseman, Mechanics of textile composites: Micro-geometry, Composites Science and Technology 68 (2008) 1671–1678.
[40] s. V. Lomov, G. Perie, d. S. Ivanov, D. Marsal, I. Verpoest, D. Marsal, Modeling three-dimensional fabrics and three-dimensional reinforced composites: Challenges and solutions, Textile Research Journal 81 (2011) 28–41.
[41] M. Blacklock, H. Bale, and Matthew Begley, B. Cox, M. Begley, B. Cox, Generating virtual textile composite specimens using statistical data from micro-computed tomography: 1D tow representations for the Binary Model, Journal of the Mechanics and Physics of Solids 60 (2012) 451–470.
[42] H. Lin, X. Zeng, M. Sherburn, A. C. Long, M. J. Clifford, Automated geometric modelling of textile structures, Textile Research Journal 82 (2012) 1689–1702.
[43] R. G. Rinaldi, M. Blacklock, H. Bale, M. R. Begley, B. N. Cox, Generating virtual textile composite specimens using statistical data from micro-computed tomography: 3D tow representations, Journal of the Mechanics and Physics of Solids 60 (2012) 1561–1581.
[44] L. Huang, Y. Wang, Y. Miao, D. Swenson, Y. Ma, C. F. Yen, Dynamic relaxation approach with periodic boundary conditions in determining the 3-D woven textile micro-geometry, Composite Structures 106 (2013) 417–425.
[45] L. Daelemans, J. Faes, S. Allaoui, G. Hivet, M. Dierick, L. Van Hoorebeke, W. Van Paepegem, Finite element simulation of the woven geometry and mechanical behaviour of a 3D woven dry fabric under tensile and shear loading using the digital element method, Composites Science and Technology 137 (2016) 177–187.
[46] M. Xu, E. Sitnikova, S. Li, Unification and parameterisation of 2D and 3D weaves and the formulation of a unit cell for composites made of such preforms, Composites Part A: Applied Science and Manufacturing 133 (2020) 105868.
[47] Q. Guo, Y. Zhang, R. Guo, X. Sun, L. Chen, Experimental and numerical study of in-plane shear properties and failure process of multiaxial 3D angle-interlock woven composites, Composite Structures 261 (2021) 113296.
[48] S. V. Lomov, A. V. Gusakov, G. Huysmans, A. Prodromou, I. Verpoest, Textile geometry preprocessor for meso-mechanical models of woven composites, Composites Science and Technology 60 (2000) 2083–2095.
[49] D. S. Ivanov, S. V. Lomov, A. E. Bogdanovich, M. Karahan, I. Verpoest, A comparative study of tensile properties of non-crimp 3D orthogonal weave and multi-layer plain weave E-glass composites. Part 2: Comprehensive experimental results, Composites Part A: Applied Science and Manufacturing 40 (2009) 1144–1157.
[50] A. Drach, B. Drach, I. Tsukrov, Processing of fiber architecture data for finite element modeling of 3D woven composites, Advances in Engineering Software 72 (2014) 18–27.

[51] B. S. F. E. Said, S. D. Green, S. R. Hallett, Kinematic modelling of 3D woven fabric deformation for structural scale features, Composites Part A: Applied Science and Manufacturing 57 (2014) 95–107.
[52] S. D. Green, A. C. Long, B. S. El Said, S. R. Hallett, Numerical modelling of 3D woven preform deformations, Composite Structures 108 (2014) 747–756.
[53] S. Li, L. F. Jeanmeure, Q. Pan, A composite material characterisation tool: UnitCells, Journal of Engineering Mathematics 95 (2015) 279–293.
[54] N. Naouar, E. Vidal-Salle, J. Schneider, E. Maire, P. Boisse, 3D composite reinforcement meso F.E. analyses based on X-ray computed tomography, Composite Structures 132 (2015) 1094–1104.
[55] I. Straumit, S. V. Lomov, M. Wevers, Quantification of the internal structure and automatic generation of voxel models of textile composites from X-ray computed tomography data, Composites Part A: Applied Science and Manufacturing 69 (2015) 150–158.
[56] B. El Said, D. Ivanov, A. C. Long, S. R. Hallett, Multi-scale modelling of strongly heterogeneous 3D composite structures using spatial Voronoi tessellation, Journal of the Mechanics and Physics of Solids 88 (2016) 50–71.
[57] S. Joglekar, M. Pankow, Modeling of 3D woven composites using the digital element approach for accurate prediction of kinking under compressive loads, Composite Structures 160 (2017) 547–559.
[58] T. Huang, Y. Gong, A multiscale analysis for predicting the elastic properties of 3D woven composites containing void defects, Composite Structures 185 (2018) 401–410.
[59] W. Huang, P. Causse, V. Brailovski, H. Hu, F. Trochu, Reconstruction of mesostructural material twin models of engineering textiles based on Micro-CT Aided Geometric Modeling, Composites Part A: Applied Science and Manufacturing 124 (2019).
[60] R. R. Madke, R. Chowdhury, A multiscale continuum model for inelastic behavior of woven composite, Composite Structures 226 (2019) 111267.
[61] Z. Ullah, X. Zhou, L. Kaczmarczyk, E. Archer, A. Mcilhagger, E. Harkin-jones, A unified framework for the multi-scale computational homogenisation of 3D-textile composites, Composites Part B 167 (2019) 582–598.
[62] M. A. Ali, Q. Guan, R. Umer, W. J. Cantwell, T. J. Zhang, Deep learning based semantic segmentation of uCT images for creating digital material twins of fibrous reinforcements, Composites Part A: Applied Science and Manufacturing 139 (2020) 106131.
[63] M. K. Dewangan, S. K. Panigrahi, Multi-scale modeling of three-dimensional angle interlock woven composite subjected to ballistic impact using FEM, Polymers for Advanced Technologies 31 (2020) 3079–3094.
[64] Z. Yang, Y. Jiao, J. Xie, L. Chen, W. Jiao, X. Li, M. Zhu, Modeling of 3D woven fibre structures by numerical simulation of the weaving process, Composites Science and Technology 206 (2021) 108679.
[65] Z. Gao, L. Chen, A review of multi-scale numerical modeling of three-dimensional woven fabric, Composite Structures 263 (2021) 113685.
[66] S. V. Lomov, Modelling the geometry of textile composite reinforcement, 2010.
[67] Y. Mahadik, S. R. Hallett, Finite element modelling of tow geometry in 3D woven fabrics, Composites Part A: Applied Science and Manufacturing 41 (2010) 1192–1200.
[68] Y. Mahadik, K. A. Brown, S. R. Hallett, Characterisation of 3D woven composite internal architecture and effect of compaction, Composites Part A: Applied Science and Manufacturing 41 (2010) 872–880.
[69] J. Bénézech, G. Couégnat, Variational segmentation of textile composite preforms from X-ray computed tomography, Composite Structures 230 (2019) 111496.
[70] A. Mendoza, J. Schneider, E. Parra, S. Roux, Measuring yarn deformations induced by the manufacturing process of woven composites, Composites Part A: Applied Science and Manufacturing 120 (2019) 127–139.
[71] A. Mendoza, J. Schneider, E. Parra, E. Obert, S. Roux, Differentiating 3D textile composites: A novel field of application for Digital Volume Correlation, Composite Structures 208 (2019) 735–743.
[72] A. Mendoza, J. Schneider, E. Parra, S. Roux, The correlation framework: Bridging the gap between modeling and analysis for 3D woven composites, Composite Structures 229 (2019) 111468.
[73] H. Moustacas, D. Durville, Y. Wielhorski, Enrichissement d'une cinématique poutre Applications aux textiles en carbone, in: 14e Colloque National en Calcul des Structures, CSMA - Giens (France) 2019, 2019, pp. 1–8.
[74] A. Mendoza, R. Trullo, Y. Wielhorski, Descriptive modeling of textiles using FE simulations and deep learning, Composites Science and Technology 213 (2021).
[75] S. Blusseau, Y. Wielhorski, Z. Haddad, S. Velasco-Forero, Instance segmentation of 3D woven fabric from tomography images by Mathematical Morphology and Deep Learning methods, 2021. Forthcoming.
[76] A. Geoffre, Y. Wielhorski, N. Moulin, J. Bruchon, S. Drapier, P.-j. Liotier, International Journal of Multiphase Flow Influence of intra-yarn flows on whole 3D woven fabric numerical permeability : from Stokes to Stokes-Darcy simulations, International Journal of Multiphase Flow 129 (2020).
[77] T. Liao, S. Adanur, A Novel Approach to Three-Dimensional Modeling of Interlaced Fabric Structures, Textile Research Journal 68 (1998) 841–847.
[78] P. Priyanka, A. Dixit, Mesoscale Numerical Characterization of Kevlar and Carbon–Kevlar Hybrid Plain-Woven Fabric Compression Behavior, Journal of Materials Engineering and Performance (2019) 5749–5762.
[79] J. Bonet, A. J. Burton, A simple orthotropic, transversely isotropic hyperelastic constitutive equation for large strain computations, Computer Methods in Applied Mechanics and Engineering 162 (1998) 151–164.
[80] A. Charmetant, E. Vidal-Sallé, P. Boisse, Hyperelastic modelling for mesoscopic analyses of composite reinforcements, Composites Science and Technology 71 (2011) 1623–1631.
[81] P. Boisse, B. Zouari, A. Gasser, A mesoscopic approach for the simulation of woven fibre composite forming, Composites Science and Technology 65 (2005) 429–436.

[82] N. Naouar, E. Vidal-Sallé, J. Schneider, E. Maire, P. Boisse, Meso-scale FE analyses of textile composite reinforcement deformation based on X-ray computed tomography, Composite Structures 116 (2014) 165–176.
[83] Y. Wang, X. Sun, Digital-element simulation of textile processes, Composites Science and Technology 61 (2001) 311–319.
[84] G. Zhou, X. Sun, Y. Wang, Multi-chain digital element analysis in textile mechanics, Composites Science and Technology 64 (2004) 239–244.
[85] D. Durville, Modélisation du comportement mécanique de câbles métalliques, Revue Europeenne des Elements 7 (1998) 9–22.
[86] D. Durville, Modélisation par éléments finis du comportement mécanique de structures textiles : de la fibre au tissu, Revue Européenne des Éléments Finis 11 (2002) 463–477.
[87] L. Daelemans, B. Tomme, B. Caglar, V. Michaud, J. Van Stappen, V. Cnudde, M. Boone, W. Van Paepegem, Kinematic and mechanical response of dry woven fabrics in through-thickness compression : Virtual fiber modeling with mesh overlay technique and experimental validation, Composites Science and Technology 207 (2021) 108706.
[88] B. Brogliato, B. Brogliato, Nonsmooth mechanics, Springer, 1999.
[89] J. J. Moreau, P. D. Panagiotopoulos, Nonsmooth mechanics and applications, volume 302, Springer, 2014.
[90] B. Ozgen, H. Gong, Modelling of yarn flattening in woven fabrics, Textile Research Journal 81 (2011) 1523–1531.
[91] T. Zheng, J. Wei, Z. Shi, T. Li, Z. Wu, An Overview of Modeling Yarn's 3D Geometric Configuration, Journal of Textile Science and Technology 01 (2015) 12–24.
[92] H. Moustacas, D. Durville, Y. Wielhorski, Modélisation et simulation par élément finis du comportement trans- verse de mèches de fibres de carbone, in: 13e Colloque National en Calcul des Structures, CSMA - Giens (France) 2017, 2017, pp. 1–8.
[93] M. Tourlonias, M. A. Bueno, C. Jordan, D. Poquillon, Influence of Wear on the Sizing Layer and Desizing of Single Carbon Fibre-to-Fibre Friction, Wear 402-403 (2018) 64–70.
[94] Y. Sugimoto, D. Shimamoto, Y. Hotta, Evaluation of kinetic friction coefficients between single carbon fibers, Carbon 167 (2020) 264–269.
[95] M. Tourlonias, M. A. Bueno, G. Fassi, I. Aktas, Y. Wielhorski, Influence of friction angle between carbon single fibres and tows: Experimental analysis and analytical model, Composites Part A: Applied Science and Manufacturing 124 (2019) 105478.
[96] M. M. Salem, E. De Luycker, K. Delbe, M. Fazzini, P. Ouagne, Experimental investigation of vegetal and synthetic fabrics cohesion in order to prevent the tow sliding defect via frictional and pull-out test, Composites Part A: Applied Science and Manufacturing 139 (2020) 106083.
[97] N. Wu, X. Xie, J. Yang, Y. Feng, Y. Jiao, L. Chen, J. Xu, X. Jian, Effect of normal load on the frictional and wear behaviour of carbon fiber in tow-on-tool contact during three-dimensional weaving process, Journal of Industrial Textiles (2020).
[98] R. H. Gong, B. Ozgen, M. Soleimani, Modeling of Yarn Cross-Section in Plain Woven Fabric, Textile Research Journal 79 (2009) 1014–1020.
[99] A. Sibellas, J. Adrien, D. Durville, E. Maire, Experimental study of the fiber orientations in single and multi-ply continuous filament yarns, Journal of the Textile Institute 111 (2020) 646–659.
[100] J. H. Byun, T.-W. Chu, Effect of yarn twist on the elastic property of composites, in: Proc. ICCM, 1995, pp. 293–299.
[101] F. Robitaille, B. R. Clayton, A. C. Long, B. J. Souter, C. D. Rudd, Geometric modelling of industrial preforms: Woven and braided textiles, Proceedings of the Institution of Mechanical Engineers Part L: Journal of Materials: Design and Applications 213 (1999) 69–83.
[102] R. Nakamura, K. Goda, Effect of yarn structure on mechanical properties of twisted yarn composites, Materials Science Forum 783-786 (2014) 1554–1559.
[103] P. Latil, L. Orgéas, C. Geindreau, P. J. Dumont, S. Rolland du Roscoat, Towards the 3D in situ characterisation of deformation micro-mechanisms within a compressed bundle of fibres, Composites Science and Technology 71 (2011) 480–488.
[104] C. P. Laurent, P. Latil, D. Durville, R. Rahouadj, C. Geindreau, L. Orgéas, J. F. Ganghoffer, Mechanical behaviour of a fibrous scaffold for ligament tissue engineering: Finite elements analysis vs. X-ray tomography imaging, Journal of the Mechanical Behavior of Biomedical Materials 40 (2014) 222–233.
[105] A. Sibellas, M. Rusinowicz, J. Adrien, D. Durville, E. Maire, The importance of a variable fibre packing density in modelling the tensile behaviour of single filament yarns, The Journal of The Textile Institute 0 (2020) 0–9.
[106] H. Lin, L. P. Brown, A. C. Long, Modelling and simulating textile structures using TexGen, in: Advanced Materials Research, volume 331, Trans Tech Publ, 2011, pp. 44–47.
[107] H. Y. Lin, A. Newton, Computer representation of woven fabric by using B-splines, Journal of the Textile Institute 90 (1999) 59–72.
[108] F. Peirce, The geometry of cloth structure., Journal Textile Institute 28 (1937) 45–96.
[109] S. Adanur, T. Liao, 3D modeling of textile composite preforms, Composites Part B: Engineering 29 (1998) 787–793.
[110] W. Shanahan, J. Hearle, An energy method for calculations in fabric mechanics. Part II: Examples of application of the method to woven fabrics., The Journal of the Textile Institute 69 (1978) 92–100.
[111] A. Kemp, An extension of peirce's cloth geometry to the treatment of nonlinear threads., Journal Textile Institute (1958) 44–48.
[112] J. Hearle, W. Shanahan, An energy method for calculations in fabric mechanics. Part I: Principles of the method., The Journal of the Textile Institute 69 (1978) 81–91.
[113] G. Hivet, P. Boisse, Consistent 3D geometrical model of fabric elementary cell. Application to a meshing preprocessor for 3D finite element analysis, Finite Elements in Analysis and Design 42 (2005) 25–49.

[114] S. V. Lomov, T. Mikolanda, M. Kosek, I. Verpoest, Model of internal geometry of textile fabrics: Data structure and virtual reality implementation, Journal of the Textile Institute 98 (2007) 1–13.
[115] J. Hofstee, F. Van Keulen, 3-D geometric modeling of a draped woven fabric, Composite Structures 54 (2001) 179–195.
[116] J. Pazmino, V. Carvelli, S. V.Lomov, S. V. Lomov, Micro-CT analysis of the internal deformed geometry of a non-crimp 3D orthogonal weave E-glass composite reinforcement, Composites Part B: Engineering 65 (2014) 147–157.
[117] P. Priyanka, H. S. Mali, A. Dixit, Geometrical Modeling and Performance Analysis of Textile Composites Using Python Scripted Software Platforms, in: Springer (Ed.), Lecture Notes on Multidisciplinary Industrial Engineering, 2020, pp. 395–405.
[118] F. Stig, S. Hallström, A modelling framework for composites containing 3D reinforcement, Composite Structures 94 (2012) 2895–2901.
[119] J. K. Dienes, On the analysis of rotation and stress rate in deforming bodies, Acta Mechanica 32 (1979) 217–232.
[120] M. Itskov, N. Aksel, A class of orthotropic and transversely isotropic hyperelastic constitutive models based on a polyconvex strain energy function, International Journal of Solids and Structures 41 (2004) 3833–3848.
[121] M. A. Khan, T. Mabrouki, E. Vidal-Sallé, P. Boisse, Numerical and experimental analyses of woven composite reinforcement forming using a hypoelastic behaviour. Application to the double dome benchmark, Journal of Materials Processing Technology 210 (2010) 378–388.
[122] A. Charmetant, J. G. Orliac, E. Vidal-Sallé, P. Boisse, Hyperelastic model for large deformation analyses of 3D interlock composite preforms, Composites Science and Technology 72 (2012) 1352–1360.
[123] E. Vidal Salle, C. Florimond, A. Charmetant, P. Boisse, Hypo- Elastic vs hyper- Elastic constitutive equation for textile materials at meso-scale, in: Key Engineering Materials, volume 611-612, 2014, pp. 243–249.
[124] S. Mathieu, Modélisation du comportement mécanique lors du procédé de mise en forme et pyrolyse des interlocks CMC, Ph.D. thesis, INSA de Lyon, 2014.
[125] J. Bonet, R. D. Wood, Nonlinear Continuum Mechanics for Finite Element Analysis, 2nd editio ed., Cambridge University Press, 2008.
[126] P. N. J. Schröder, On the Construction of Polyconvex Anisotropic Free Energy Functions, Miehe C. (eds) IUTAM Symposium on Computational Mechanics of Solid Materials at Large Strains. Solid Mechanics and Its Applications 108 (2003) 171–180.
[127] J. M. Ball, Convexity conditions and existence theorems in nonlinear elasticity, Archive for Rational Mechanics and Analysis 63 (1976) 337–403.
[128] Q. S. Zheng, Theory of representations for tensor functions-a unified invariant approach to constitutive equations, Applied Mechanics Reviews 47 (1994) 545–587.
[129] H. Xiao, O. T. Bruhns, A. Meyers, Hypo-Elasticity Model Based upon the Logarithmic Stress Rate, Journal of Elasticity 47 (1997) 51–68.
[130] B. Hagege, Simulation du comportement mécanique des milieux fibreux en grandes transformations : Application aux renforts tricotés, Ph.D. thesis, Université d'Orléans, 2004.
[131] D. Durville, Simulation of the mechanical behaviour of woven fabrics at the scale of fibers, International Journal of Material Forming 3 (2010) 1241–1251.
[132] H. Moustacas, Modélisation et simulation du comportement de mèches de fibres de carbone à l' échelle mésoscopique pour l'analyse du comportement de préformes tissées interlock, Ph.D. thesis, CentraleSupelec, 2019.
[133] S. Green, A. Long, S. Hallett, Simulated textile geometry with realistic deformations for finite element modelling, in: TEXCOMP-11, Leuven, 2013, pp. 2–7.
[134] Y. Gofman, Outline of a set of points, Pattern Recognition Letters 14 (1993) 31–38.
[135] F. Bernardini, J. Mittleman, H. Rushmeier, C. Silva, G. Taubin, The ball-pivoting algorithm for surface reconstruction, IEEE Transactions on Visualization and Computer Graphics 5 (1999) 349–359.
[136] A. Charmetant, Approches hyperélastiques pour la modélisation du comportement mécanique de préformes tissées de composites, Ph.D. thesis, INSA Lyon, 2011.
[137] A. Iwata, T. Inoue, N. Naouar, P. Boisse, S. V. Lomov, Coupled meso-macro simulation of woven fabric local deformation during draping, Composites Part A: Applied Science and Manufacturing 118 (2019) 267–280.
[138] M. Ghazimoradi, N. Naouar, V. Carvelli, P. Boisse, Numerical modelling of the mechanical behaviour of tetraxial technical textiles, Journal of Materials Science 54 (2019) 3632–3647.
[139] A. Gasser, P. Boisse, S. Hanklar, Mechanical behaviour of dry fabric reinforcements. 3D simulations versus biaxial tests, Computational Materials Science 17 (2000) 7–20.
[140] E. Vidal-Sallé, P. Badel, E. Maire, S. Gatouillat, P. Boisse, Simulation et analyse par tomographie X de la déformation à l'échelle mésoscopique de renforts textiles de composites en cours de mise en forme = Simulation and tomography analyses of textile composite reinforcement deformation during forming, in: 16e Journées Nationales sur les Composites, Toulouse, 2009, pp. 1–8.
[141] C. Florimond, Contributions à la modélisation mécanique du comportement de mèches de renforts tissés à l'aide d'un schéma éléments finis implicite, Ph.D. thesis, Institut National des Sciences Appliquées de Lyon, 2013.
[142] S. Gatouillat, A. Barregi, E. Vidal-Sallé, P. Boisse, Simulation of composite forming at meso scale, Key Engineering Materials 554-557 (2013) 410–415.
[143] J. Xie, X. Chen, Y. Zhang, G. Fang, L. Chen, Experimental and numerical investigation of the needling process for quartz fibers, Composites Science and Technology 165 (2018) 115–123.
[144] M. Ghaedsharaf, J.-E. Brunel, L. L. Lebel, Fiber-level numerical simulation of biaxial braids for mesoscopic morphology prediction validated by X-ray computed tomography scan, Composites Part B: Engineering 218 (2021) 108938.
[145] C. Bessette, M. Decrette, M. Tourlonias, J. F. Osselin, F. Charleux, D. Coupé, M. A. Bueno, In-situ measurement of

tension and contact forces for weaving process monitoring: Application to 3D interlock, Composites Part A: Applied Science and Manufacturing 126 (2019) 105604.
[146] S. V. Lomov, I. Verpoest, J. Cichosz, C. Hahn, D. S. Ivanov, B. Verleye, Meso-level textile composites simulations: Open data exchange and scripting, Journal of Composite Materials 48 (2014) 621–637.
[147] S. V. Lomov, G. Huysmans, I. Verpoest, Hierarchy of Textile Structures and Architecture of Fabric Geometric Models, Textile Research Journal 71 (2001) 534–543.
[148] I. Verpoest, S. V. Lomov, Virtual textile composites software WiseTex: Integration with micro-mechanical, permeability and structural analysis, Composites Science and Technology 65 (2005) 2563–2574.
[149] F. Robitaille, B. Clayton, A. Long, B. Souter, C. Rudd, A geometrical model for textile preforms, in: 19th SAMPE Europe International Conference, Paris, France, 1998, p. 151–62.
[150] F. Robitaille, B. R. Clayton, A. C. Long, B. J. Souter, C. D. Rudd, Geometric modelling of industrial preforms: Warp-knitted textiles, Proceedings of the Institution of Mechanical Engineers Part L: Journal of Materials: Design and Applications 214 (2000) 71–90.
[151] L. Adam, R. Assaker, Integrated nonlinear multi-scale material modelling of fiber reinforced plastics with digimat: Application to short and continuous fiber composites, 11th World Congress on Computational Mechanics, 5th European Conference on Computational Mechanics, 6th European Conference on Computational Fluid Dynamics, ECFD 2014 (2014) 2322–2333.
[152] S. V. Lomov, D. S. Ivanov, G. Perie, I. Verpoest, Modelling 3D fabrics and 3D-reinforced composites: Challenges and solutions, in: 1st World Conference on 3D Fabrics, 1-1, 2008, pp. 1–16.
[153] B. Wucher, S. Hallström, D. Dumas, T. Pardoen, C. Bailly, P. Martiny, F. Lani, Nonconformal mesh-based finite element strategy for 3D textile composites, Journal of Composite Materials 51 (2016) 2315–2330.
[154] M. A. Ali, R. Umer, K. A. Khan, S. Bickerton, W. J. Cantwell, Non-destructive evaluation of through-thickness permeability in 3D woven fabrics for composite fan blade applications, Aerospace Science and Technology 82 (2018) 520–533.
[155] M. A. Ali, R. Umer, K. A. Khan, W. J. Cantwell, XCT-scan assisted flow path analysis and permeability prediction of a 3D woven fabric, Composites Part B: Engineering 176 (2019) 107320.
[156] M. A. Ali, R. Umer, K. A. Khan, W. J. Cantwell, In-plane virtual permeability characterization of 3D woven fabrics using a hybrid experimental and numerical approach, Composites Science and Technology 173 (2019) 99–109.
[157] Y. Liu, I. Straumit, D. Vasiukov, S. V. Lomov, S. Panier, Prediction of linear and non-linear behavior of 3D woven composite using mesoscopic voxel models reconstructed from X-ray micro-tomography, Composite Structures 179 (2017) 568–579.
[158] J. Bigun, G. H. Granlund, Optimal Orientation Detection of Linear Symmetry., Proceedings of the IEEE First International Conference on Computer Vision (1987) 433–438.
[159] J. Bigun, T. Bigun, K. Nilsson, Recognition by symmetry derivatives and the generalized structure tensor, IEEE Transactions on Pattern Analysis and Machine Intelligence 26 (2004) 1590–1605.
[160] J. Bigün, J. M. Hans du buf, N-folded Symmetries by Complex Moments in Gabor Space and Their Application to Unsupervised Texture Segmentation, IEEE Transactions on Pattern Analysis and Machine Intelligence 16 (1994) 80–87.
[161] B. Wintiba, D. Vasiukov, S. Panier, S. V. Lomov, K. Ehab Moustafa Kamel, T. J. Massart, Automated reconstruction and conformal discretization of 3D woven composite CT scans with local fiber volume fraction control, Composite Structures 248 (2020) 112438.
[162] T. Löfstedt, P. Brynolfsson, T. Asklund, T. Nyholm, A. Garpebring, Gray-level invariant Haralick texture features, PLoS ONE 14 (2019) 1–18.
[163] R. M. Haralick, K. Shanmugam, I. H. Dinstein, Textural features for image classification, IEEE Transactions on systems, man, and cybernetics 6 (1973) 610–621.
[164] M. Ali, Q. Guan, R. Umer, W. J. Cantwell, T. Zhang, Efficient processing of uct images using deep learning tools for generating digital material twins of woven fabrics, Composites Science and Technology 217 (2022) 109091.
[165] L. C. Chen, Y. Zhu, G. Papandreou, F. Schroff, H. Adam, Encoder-decoder with atrous separable convolution for semantic image segmentation, Lecture Notes in Computer Science (including subseries Lecture Notes in Artificial Intelligence and Lecture Notes in Bioinformatics) 11211 LNCS (2018) 833–851.
[166] K. He, X. Zhang, S. Ren, J. Sun, Deep residual learning for image recognition, in: Proceedings of the IEEE Computer Society Conference on Computer Vision and Pattern Recognition, volume 2016-Decem, 2016, pp. 770–778.
[167] O. Russakovsky, J. Deng, H. Su, J. Krause, S. Satheesh, S. Ma, Z. Huang, A. Karpathy, A. Khosla, M. Bernstein, A. C. Berg, L. Fei-Fei, ImageNet Large Scale Visual Recognition Challenge, International Journal of Computer Vision 115 (2015) 211–252.
[168] O. Ronneberger, P. Fischer, T. Brox, U-Net: Convolutional networks for biomedical image segmentation, in: Lecture Notes in Computer Science (including subseries Lecture Notes in Artificial Intelligence and Lecture Notes in Bioinformatics), volume 9351, Springer, 2015, pp. 234–241.
[169] A. Ewert, B. Drach, K. Vasylevskyi, I. Tsukrov, Predicting the overall response of an orthogonal 3D woven composite using simulated and tomography-derived geometry, Composite Structures 243 (2020) 112169.
[170] B. Wintiba, B. Sonon, K. Ehab Moustafa Kamel, T. J. Massart, An automated procedure for the generation and conformal discretization of 3D woven composites RVEs, Composite Structures 180 (2017) 955–971.
[171] D. G. Kirkpatrick, R. Seidel, On the Shape of a Set of Points in the Plane, IEEE Transactions on Information Theory 29 (1983) 551–559.
[172] K. He, G. Gkioxari, P. Dollár, R. Girshick, Mask R-CNN, in: 2017 IEEE International Conference on Computer Vision (ICCV), 2017, pp. 2980–2988.